JPCAFH

APRIL 24, 2014
VOLUME 118
NUMBER 16
pubs.acs.org/JPCA

THE JOURNAL OF PHYSICAL CHEMISTRY A

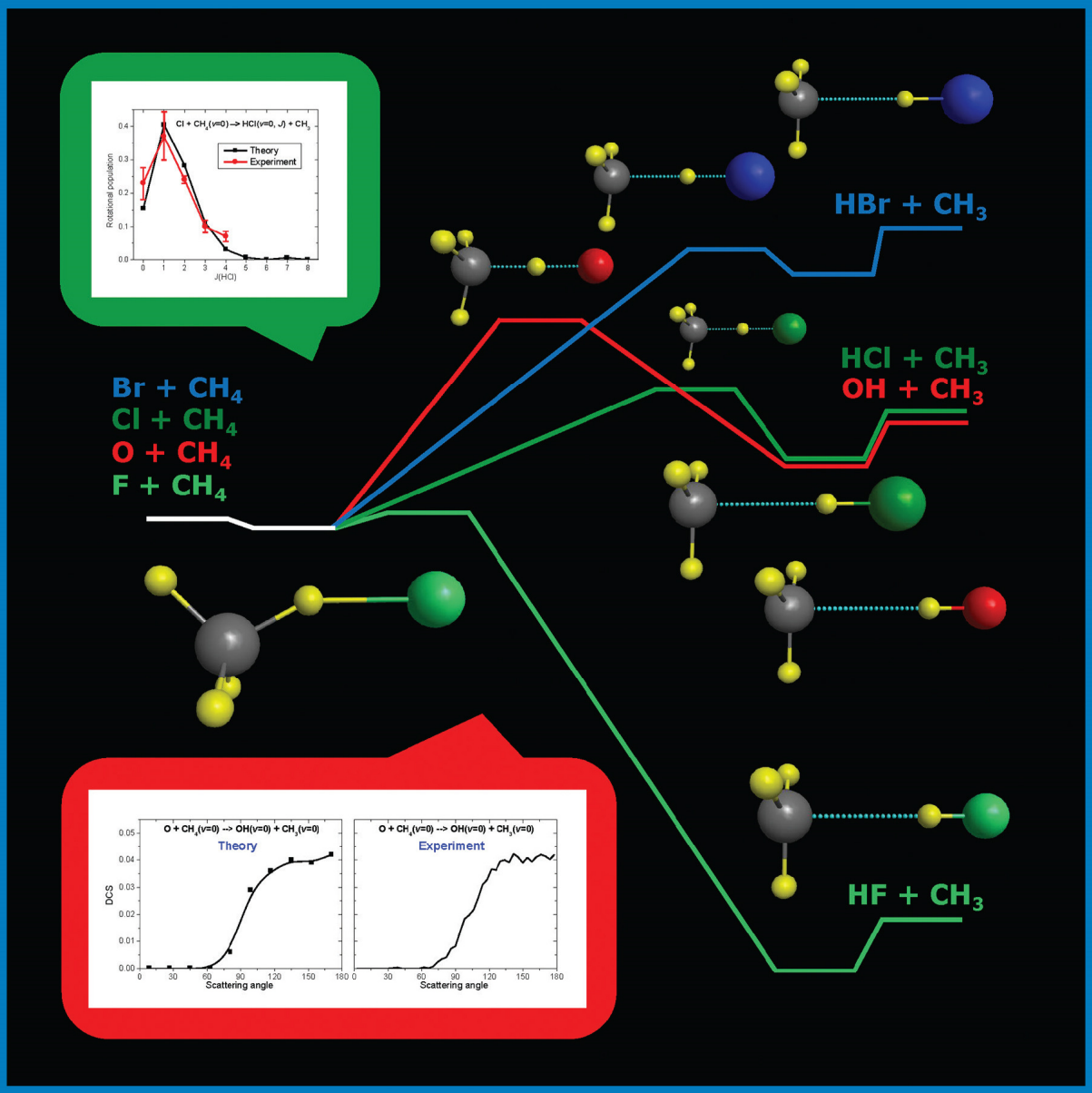

Schematic of the Energies of Indicated X + CH_4 Reactions from *ab Initio* Potential Surfaces (see page 5A)

ISOLATED MOLECULES, CLUSTERS, RADICALS, AND IONS; ENVIRONMENTAL CHEMISTRY, GEOCHEMISTRY, AND ASTROCHEMISTRY; THEORY

ACS Publications
Most Trusted. Most Cited. Most Read.

www.acs.org

THE JOURNAL OF PHYSICAL CHEMISTRY A

Feature Article

pubs.acs.org/JPCA

Reaction Dynamics of Methane with F, O, Cl, and Br on ab Initio Potential Energy Surfaces

Gábor Czakó*,† and Joel M. Bowman*,‡

†Laboratory of Molecular Structure and Dynamics, Institute of Chemistry, Eötvös University, H-1518 Budapest 112, P.O. Box 32, Hungary

‡Cherry L. Emerson Center for Scientific Computation and Department of Chemistry, Emory University, Atlanta, Georgia 30322, United States

ABSTRACT: The bimolecular hydrogen abstraction reactions of methane with atoms have become benchmark systems to test and extend our knowledge of polyatomic chemical reactivity. We review the state-of-the-art methodologies for reaction dynamics computations of X + methane [X = F, O(^{3}P), Cl, Br] reactions, which consist of two key steps: (1) potential energy surface (PES) developments and (2) reaction dynamics computations on the PES using either classical or quantum methods. We briefly describe the permutationally invariant polynomial approach for step 1 and the quasiclassical trajectory method, focusing on the mode-specific polyatomic product analysis and the Gaussian binning (1GB) techniques, and reduced-dimensional quantum models for step 2. High-quality full-dimensional ab initio PESs and dynamical studies of the X + CH_4 and CHD_3 reactions are reviewed. The computed integral cross-sections, angular, vibrational, and rotational product distributions are compared with available experiments. Both experimental and theoretical findings shed light on the rules of mode-selective polyatomic reactivity.

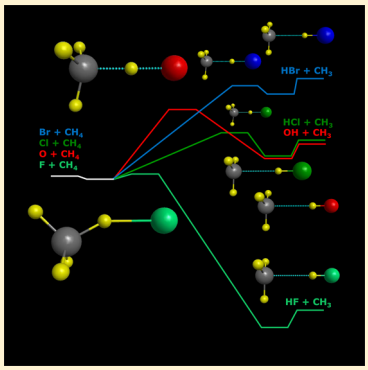

I. INTRODUCTION

Since the first three-dimensional quantum mechanical study of the dynamics of the H + H_2 reaction reported by Schatz and Kuppermann[1] in 1975, reaction dynamics has become a growing field of chemical sciences driven by the close interaction between theory and experiment. In the early years atom + diatom reactions, such as H, F, and Cl + H_2, received a lot of attention.[2−4] This class of reactions is often referred as A + BC, and the so-called ABC code[5] is routinely used nowadays for quantum reactive scattering computations for A + BC systems. Many experiences with atom + diatom reactions, accumulated mainly using quasiclassical trajectory (QCT) calculations, resulted in the Polanyi rules,[6] which are the rules of thumb of reaction dynamics. The rules say that the location of the barrier that separates the reactants from the products determines the relative efficacy of translational and vibrational energy on the reactivity. For early barrier reactions (the transition state has a reactant-like structure), the relative translational energy of the reactants is more efficient than vibrational excitation to activate the reaction, whereas the reverse holds for late-barrier reactions. The extension of these rules for polyatomic systems may not be so simple due to the increasing number of vibrational degrees of freedom, which may involve the concerted motion of many atoms.

In order to investigate the dynamics of more complex systems the diatomic reactant was replaced by polyatomic molecules. The reaction of water (H_2O, HOD, and D_2O) with hydrogen (H and D) atom became a prototype of polyatomic bimolecular reactions.[7−11] Furthermore, the H + HOD reaction became probably the first example of mode- and bond-selective chemistry, a topic of exceptional importance, since selectively breaking chemical bonds has always been the dream of chemists. The mode-selectivity in H + HOD was first predicted in 1984 by the early QCT calculations of Schatz and co-workers.[7] They found that a five-quantum excitation of the OH stretching mode enhances the reactivity by a factor of 10−10^3 relative to the OD stretching excited H + HOD → H_2 + OD reaction.[7] In the early 1990s bond-selective experiments were performed for the H + HOD reaction in the groups of Crim[8,10] and Zare,[9] and these measurements confirmed the previous theoretical predictions.[7] In 1997 Zhang and Light[10] carried out quantum dynamics computations for H + HOD showing that one-quantum excitation of the OH-stretch gives a 13.5:1 OD/OH product ratio, whereas excitation of the OD-stretch gives an OD/OH ratio of 1:5, in qualitative agreement with experiment of Zare and co-workers.[9]

In the early 2000s reaction dynamics studies started to investigate the atom + methane (CH_4, CHD_3, etc.) hydrogen abstraction reactions.[12−15] These are the simplest reactions of a tetrahedral organic molecule, but the dynamics can be quite complex because methane has nine vibrational modes including various torsional, bending, and stretching motions. Does the excitation of every vibrational mode have the same effect on reactivity? Can the Polanyi rules simply be extended for atom + methane reactions? These fundamental questions, among others, motivated both theoretical and experimental chemists to investigate the dynamics of atom + methane reactions. In the

Received: January 4, 2014
Revised: February 16, 2014
Published: March 5, 2014

recent years X + CH_4 abstraction reactions have become benchmark systems to study polyatomic reactivity. The kinetics and dynamics of the H + CH_4 reaction, which has been probably the most thoroughly studied X + CH_4 reaction, were reviewed in detail in ref 16. In the present Feature Article, we describe the recent progress on the dynamics of the X + CH_4 [X = F, O(^{3}P), Cl, Br] reactions focusing on our theoretical contributions and mentioning, of course, many other theoretical work and experiments. Note that the other important class of six-atom bimolecular reactions, that is the X^- + CH_3Y nucleophilic substitution (S_N2) reactions, was recently reviewed by Hase and co-workers.[17]

Following the pioneering Cl + methane experiments of Zare et al.[13] and Crim et al.,[14] in 2003 Liu and co-workers[15] developed a novel experimental technique to measure the pair-correlated coincident product vibrational states in the F + $CD_4 \rightarrow DF(v)$ + $CD_3(n_1n_2n_3n_4)$ reaction. These state-to-state correlated vibrational distributions allowed tracking the energy flow along the reaction coordinate. In the past 10 years Liu and co-workers applied this technique to the F, Cl, and O(^{3}P) + methane reactions and uncovered departures from our expectations based on A + BC systems.[18−21] In 2009 they found that the CH stretching excitation inhibits the cleavage of the CH bond in the F + CHD_3 reaction.[19] In 2007 experiment showed that CH stretching excitation is no more efficient than translational energy to activate the late-barrier Cl + CHD_3 reaction,[18] in contradiction to the extended Polanyi rules. In 2010, experiment revealed that the CH stretching excitation enlarges the reactive cone of acceptance in the O + CHD_3 reaction, thereby providing the mechanistic origin of the enhancement of the OH + CD_3 channel upon reactant CH stretching excitation.[20]

The theoretical simulation of the X + methane reactions consists of two key steps. First, one has to solve the Schrödinger equation of the electrons at fixed nuclear configurations, which provides the potential energy surface (PES). Second, dynamical computations have to be performed on the PES using either classical or quantum mechanical methods.

Potential energies can be computed on-the-fly using an electronic structure program whenever they are needed during a dynamics computation. This approach in connection with classical dynamics is usually called direct dynamics or ab initio molecular dynamics. Since a quantitative classical trajectory study requires millions of potential energies and gradients, usually direct dynamics computations can only afford using relatively low-level electronic structure methods. It is worth noting that for the F and Cl + methane reactions Troya and co-workers[22,23] developed reaction-specific semiempirical Hamiltonians that allow efficient direct dynamics computations. Another approach represents the PES by an analytical function that can be evaluated highly efficiently during the reaction dynamics computations.[24−30,16] For the F, O, Cl, and Br + methane reactions, Espinosa-García and co-workers[31−34] developed semiempirical PESs by modifying the parameters of a well-known analytical function[35] designed for the H + CH_4 reaction. These semiempirical PESs were usually calibrated against available experimental data, e.g., rate constants and reaction enthalpies, and equilibrium and saddle-point ab initio results. A fully ab initio approach using high-level energies to obtain a PES is clearly desirable. We have taken this approach to fit scattered ab initio energy points, which cover the energy range and configuration space of chemical importance.[29,30,16] The fitting method explicitly incorporates the permutational invariance of like atoms; it has been previously reviewed in detail in refs 29 and 16. In section II, we just briefly summarize the key details of the permutationally invariant PES development, which played an essential part in the dynamical investigations of the X + methane reactions. Beside our PESs, ab initio PESs have been constructed using the Shepard interpolation method for the F and Cl + methane reactions.[36,37]

Full-dimensional, quantum state-to-state dynamics computations for six-atom systems are not feasible at present; therefore, quasi-classical trajectory and reduced-dimensional quantum dynamical methods have been applied to the X + methane reactions. (Note, however, that Manthe and co-workers have made great progress toward full-dimensional rate constant calculations of X + methane reactions using the multiconfiguration time-dependent Hartree[38] (MCTDH) approach.[39] Furthermore, Suleimanov and co-workers successfully applied the full-dimensional ring polymer molecular dynamics (RPMD) approach to rate computations of X + CH_4 systems.[40,41]) In section II, we briefly review the QCT method focusing on the polyatomic mode-specific product analysis method and the novel binning techniques applied to obtain quantized vibrational distributions. Then we summarize the reduced-dimensional quantum models used for X + methane reactions. In section III, the computational details and properties of the full-dimensional ab initio PESs of the X + CH_4 [X = F, O, Cl, Br] reactions are described, and the computed dynamical results are discussed and compared with the available experimental findings.

II. METHODS

A. Potential Energy Surfaces. We represent the potential energy surface by an analytical function obtained by fitting accurate ab initio energy points. In order to achieve the correct asymptotic behavior, we use Morse-type variables, i.e., $y_{ij} = \exp(-r_{ij}/a)$, where r_{ij} denote the interatomic distance and a is a fixed parameter, typically 2 or 3 bohr. The functional form of the PES can be given in terms of all the internuclear y_{ij} variables as[29,16]

$$V = \sum_{\mathbf{n}=\mathbf{0}}^{\mathbf{N}} C_{\mathbf{n}} S(y_{12}^{n_1} y_{13}^{n_2} y_{14}^{n_3} \cdots y_{23}^{n_j} y_{24}^{n_k} \cdots) \tag{1}$$

where S is a symmetrization operator and $C_{\mathbf{n}}$ are linear coefficients obtained by a standard weighted linear least-squares fitting method. The symmetrization ensures that the fitting basis is explicitly invariant under permutation of identical atoms. We usually apply a simple weight function of $E_0/(E + E_0)$, where E is the potential energy relative to the global minimum and E_0 is a parameter chosen to be around 0.05−0.1 E_h. The overall maximum power of symmetrized monomials is constrained at typically 5 or 6.

The theory of invariant polynomials offers an elegant and efficient way to represent PESs as[29,16]

$$V(\mathbf{y}) = \sum_{n=0}^{N} h_n[\mathbf{p}(\mathbf{y})] q_n(\mathbf{y}) \tag{2}$$

where h_n is a polynomial of the primary invariant polynomials, $\mathbf{p}(\mathbf{y})$ and $q_n(\mathbf{y})$ are secondary invariant polynomials, and $\mathbf{y}$ represents the set of variables y_{ij}. In practical applications we use this sophisticated approach for PES developments since eq 2 allows efficient implementation. Detailed descriptions on the monomial symmetrization approach and the invariant polynomial theory can be found in previous reviews.[29,16] The practical details relevant to the X + methane systems will be given in section III.

B. Quasiclassical Trajectory Calculations. The QCT method is frequently used to study the atomic level dynamics and mechanisms of chemical reactions in the gas phase. QCT employs special quasiclassical initial conditions for the trajectories in which each reactant has internal energy initial state-selection corresponding to that of a specific ro-vibrational state. Then the trajectories are propagated using standard classical mechanics where the negative gradients of the PES give the forces. Therefore, the efficiency of the potential gradient computations determines the computational cost of the QCT calculations. If an analytical PES is available, the potential energies and gradients can be evaluated highly efficiently, thereby allowing running millions of trajectories for six-atom systems. A detailed review of the QCT method for polyatomic reactants was published by Hase in 1998.[42] Below we focus on the initial conditions relevant for the X + methane reactions that we have used in our own software, and we present the details of the recent method developments for the mode-specific vibrational analysis of polyatomic products.

1. Initial Conditions. Standard normal-mode sampling is employed to prepare the initial quasiclassical vibrational ground and mode-specific excited states. The normal coordinates and momenta are obtained for an N-atom system as

$$Q_k = \frac{\sqrt{2E_k}}{\omega_k}\cos(2\pi R_k) \quad P_k = -\sqrt{2E_k}\,\sin(2\pi R_k)$$
$$k = 1, 2, ..., 3N - 6 \tag{3}$$

where $R_k \in [0, 1]$ is a random number, ω_k denotes the harmonic frequencies, and the energy of each mode is $E_k = (n_k + 1/2)\omega_k$. The quasiclassical ground state can be prepared by setting each vibrational quantum number, n_k, to zero. One can also prepare mode-specific excited vibrational states by giving the appropriate integer value for the specific n_k. Then the normal coordinates and momenta are transformed into the Cartesian space, and any spurious angular momentum is subtracted by standard modifications of the velocities. Then, as described in detail in ref 42, a tuning procedure is applied to set the actual internal energy computed using the correct anharmonic Hamiltonian in the Cartesian space to be equal with the intended energy of $\sum_{k=1}^{3N-6} E_k$.

The initial distance between the center of mass of the reactants is $(x^2 + b^2)^{1/2}$, where b is the impact parameter and x is usually around 10 bohr. The orientation of methane is randomly sampled and b is scanned from 0 to b_{max} using an equidistant grid. The maximum impact parameter, b_{max}, is usually 6−7 bohr for the X + methane reactions. We compute roughly 5000 trajectories, or 25 000 if the reactivity is small, at each b; resulting in a total number of trajectories roughly a hundred thousand for each collision energy (E_{coll}). In our X + methane studies, an integration step of 0.0726 fs (3 atomic time unit) is used, and the trajectories usually finish within a few hundred fs.

Since we run trajectories at equidistant fixed b values, the final cross-sections are obtained by a b-weighted integration of the reaction probabilities, $P(b)$, as

$$\sigma = \pi \sum_{n=1}^{n_{max}} [b_n - b_{n-1}][b_n P(b_n) + b_{n-1} P(b_{n-1})] \tag{4}$$

where $b_n = n \times d$ $[n = 0, 1, ..., n_{max}]$ and d is typically 0.5 bohr or less. It is also possible to sample b as $b = (R)^{1/2} b_{max}$, where R is a random number between 0 and 1, and then the cross-section is obtained simply as $\sigma = N_r/N_{tot}\pi b_{max}^2$, where N_r is the number of the reactive trajectories from the total number of trajectories (N_{tot}). We also calculate differential cross-sections, and to achieve good precision, we prefer the equal space sampling of b. Note that the two different b sampling approaches converge to the same final results as the number of trajectories increases and the b spacing decreases.

2. Mode-Specific Vibrational Product Analysis. Motivated by the measurements of vibrationally state-specific correlated product distributions for the F, Cl, and O + methane reactions,[15,18−20] method developments for the determination of the classical actions of polyatomic products obtained from QCTs were desired. Semiclassical quantization was successfully applied to triatomic molecules;[43] however, the use of the semiclassical method for larger products was found impractical. Therefore, a more straightforward and robust normal-mode analysis method was proposed by Espinosa-García and co-workers[44] and also by us.[45,46] This normal-mode product analysis approach is reviewed below.

The first step of the procedure is to relate the final configuration, with Cartesian coordinates denoted by $\mathbf{r}_i$ (i = 1, 2, ..., N), of the N-atomic product to normal mode displacements of a reference minimum geometry (denoted as $\mathbf{r}_i^{eq}$). There are different ways to find the reference geometry in the Cartesian space. (1) We can initiate a gradient-based geometry optimization procedure from $\mathbf{r}_i$ to locate the closest minimum without introducing significant overall rotation in the Cartesian space. This method can be useful when the minimum energy structure is unknown a priori and/or multiple minima exist on the PES. This is the case in liquids and solids, where Stillinger and Weber[47] used a steepest descent method to assign configurations to a particular minimum. This quenching method was successfully applied by us to the methyl product of the F + CHD_3 reaction in 2009.[45] (2) Of course, for small systems the relevant minimum energy structure is usually known a priori; thus, one just needs to find the optimal orientation of $\mathbf{r}_i$ with respect to $\mathbf{r}_i^{eq}$. This can be done by finding the best overlap between $\mathbf{r}_i$ and $\mathbf{r}_i^{eq}$ by minimizing

$$\sum_{i=1}^{N} \| \mathbf{C}(\theta, \phi, \psi)\mathbf{r}_i - \mathbf{r}_i^{eq} \|^2 \tag{5}$$

with respect to the three Euler angles as was done in refs 48−52. Recently in ref 46, the solution of

$$\sum_{i=1}^{N} m_i \mathbf{r}_i^{eq} \times (\mathbf{C}(\theta, \phi, \psi)\mathbf{r}_i - \mathbf{r}_i^{eq}) = \mathbf{0} \tag{6}$$

was proposed, thereby satisfying the rotational Eckart condition.[53] A general solution for satisfying eq 6 was reported by Dymarsky and Kudin,[54] and here we present our practical implementation, which was first described in ref 46.

(1) Let us denote center-of-mass Cartesian coordinates, center-of-mass Cartesian velocities, and masses of the N-atomic product molecule as $\mathbf{r}_i$, $\mathbf{v}_i$, and m_i, (i = 1, 2, ..., N), respectively. Suppose we know the equilibrium structure of the product molecule in *any* orientation in the center of mass frame (denoted as $\mathbf{r}_i^{eq}$). We perform a normal-mode analysis in $\mathbf{r}_i^{eq}$, which provides, in the case of nonlinear equilibrium structure, 3N−6 nonzero harmonic frequencies ω_k and the orthogonal transformation matrix $\mathbf{l} \in \mathcal{R}^{(3N-6)\times 3N}$, which transforms from mass-scaled Cartesian coordinates to normal coordinates. This normal-mode analysis is done only *once* at the beginning of the product analysis, and the same reference structure and $\mathbf{l}$ matrix are used for every trajectory. For each trajectory, $\mathbf{r}_i$ and $\mathbf{v}_i$ are

rotated to the Eckart frame corresponding to reference geometry $\mathbf{r}_i^{eq}$. Thus, the steps discussed below must be repeated for each reactive trajectory.

(2) We remove the angular momentum by modifying velocities as

$$\mathbf{v}_i^{nr} = \mathbf{v}_i - \mathbf{\Omega} \times \mathbf{r}_i \tag{7}$$

where $\mathbf{\Omega} = \mathbf{I}^{-1}\mathbf{j}$, where $\mathbf{I}^{-1}$ is the inverse of the moment of inertia tensor at $\mathbf{r}_i$ and $\mathbf{j} = \sum_{i=1}^{N} \mathbf{r}_i \times (m_i\mathbf{v}_i)$.

(3) The matrix $\mathbf{C}$, which transforms to the Eckart frame, is obtained as follows:

$$A_{n,m} = \sum_{i=1}^{N} m_i r_{i,n} r_{i,m}^{eq} \quad n, m = 1(x), 2(y), 3(z) \tag{8}$$

$$\mathbf{A}_1 = \mathbf{A}^T\mathbf{A} \text{ and } \mathbf{A}_2 = \mathbf{A}\mathbf{A}^T \tag{9}$$

$$\mathbf{C} = \mathbf{U}_1\mathbf{U}_2^T \tag{10}$$

where the columns of $\mathbf{U}_1$ and $\mathbf{U}_2$ contain the normalized eigenvectors of the real symmetric matrices $\mathbf{A}_1$ and $\mathbf{A}_2$, respectively. The Cartesian coordinates, which exactly satisfy the Eckart conditions and the corresponding velocities are obtained as $\mathbf{C}\mathbf{r}_i$ and $\mathbf{C}\mathbf{v}_i^{nr}$, respectively. Before we move forward it is important to consider the fact that the sign of an eigenvector is not well-defined; therefore, eight different $\mathbf{C}$ matrices exist, which all satisfy the Eckart conditions. The $\mathbf{C}$ matrix of interest is obtained by finding the best overlap between $\mathbf{C}\mathbf{r}_i$ and $\mathbf{r}_i^{eq}$ as described in detail in ref 46.

(4) The coordinates and momenta in the normal mode space are obtained as

$$Q_k = \sum_{i=1}^{N} \sqrt{m_i}\mathbf{l}_{ki}(\mathbf{C}\mathbf{r}_i - \mathbf{r}_i^{eq}) \quad P_k = \sum_{i=1}^{N} \sqrt{m_i}\mathbf{l}_{ki}\mathbf{C}\mathbf{v}_i^{nr}$$
$$k = 1, 2, ..., 3N - 6 \tag{11}$$

(5) The harmonic vibrational energy for each normal mode is calculated as

$$E_k = \frac{P_k^2}{2} + \frac{\omega_k^2 Q_k^2}{2} \quad k = 1, 2, ..., 3N - 6 \tag{12}$$

(6) A noninteger classical harmonic action for each mode is obtained as

$$n_k' = \frac{E_k}{\omega_k} - \frac{1}{2} \quad k = 1, 2, ..., 3N - 6 \tag{13}$$

The integer vibrational quanta are assigned to quantum states by rounding n_k' to the nearest integer value n_k. Hereafter we denote a vibrational state $(n_1, n_2, ..., n_{3N-6})$ as $\mathbf{n}$.

3. Binning Techniques. The standard QCT studies apply the histogram binning (HB) technique, where the probability of a particular vibrational state $\mathbf{n}$ is

$$P_{HB}(\mathbf{n}) = \frac{N(\mathbf{n})}{N_{tot}} \tag{14}$$

where $N(\mathbf{n})$ is the number of products in state $\mathbf{n}$ from the total number of trajectories N_{tot}.

In order to incorporate the quantum spirit into the QCT product analysis, the Gaussian binning (GB) method was proposed by Bonnet and co-workers.[55,56] GB was successfully applied for diatomic products;[57−59] however, the efficient application of GB to polyatomic products was problematic due to the exponential scaling of the computational effort with the number of the vibrational modes. In 2009 we proposed to compute the Gaussian weight for each product based on the total vibrational energy as[45]

$$G_p(\mathbf{n}) = \frac{\beta}{\sqrt{\pi}} e^{-\beta^2\left(\frac{E(\mathbf{n}_p') - E(\mathbf{n})}{2E(\mathbf{0})}\right)^2} \quad p = 1, 2, ..., N(\mathbf{n}) \tag{15}$$

where $\beta = 2(\ln 2)^{1/2}/\delta$, δ is the full-width at half-maximum, and $E(\mathbf{0})$ is the harmonic zero-point energy (ZPE). Then, the probability of $\mathbf{n}$ can be obtained as

$$P_{GB}(\mathbf{n}) = \frac{\sum_{p=1}^{N(\mathbf{n})} G_p(\mathbf{n})}{N_{tot}} \tag{16}$$

In 2010 Bonnet and Espinosa-García[60] reported some theoretical arguments proving the accuracy of eq 15, which is now called 1GB. Several recent applications showed the utility of 1GB for $X + CH_4 \rightarrow HX + CH_3$ [X = F, Cl, O],[45,61,62] $Cl + CH_4 \rightarrow H + CH_3Cl$,[46] $(H_2O)_2 \rightarrow 2H_2O$,[50,52] $OH + D_2 \rightarrow D + HOD$,[63,64] $OH + CO \rightarrow H + CO_2$,[65] and $OH^* + H_2 \rightarrow H + H_2O$,[66] and their isotopologue−analogue reactions.

Now let us consider three different ways to calculate $G_p(\mathbf{n})$ by using different approaches to obtain the energies $E(\mathbf{n}_p')$ and $E(\mathbf{n})$ used in eq 15.

(1) As we proposed originally in 2009,[45] one can use the harmonic energy formulas for both $E(\mathbf{n}_p')$ and $E(\mathbf{n})$ as follows:

$$E(\mathbf{n}_p') = \sum_{k=1}^{3N-6} \omega_k\left(\mathbf{n}_{k,p}' + \frac{1}{2}\right) \tag{17}$$

and

$$E(\mathbf{n}) = \sum_{k=1}^{3N-6} \omega_k\left(n_k + \frac{1}{2}\right) \tag{18}$$

A possible issue of this approach is that the harmonic normal mode approximation may fail at highly distorted configurations, and thus, $E(\mathbf{n}_p')$ may be seriously overestimated.

(2) One can overcome the above-mentioned issue by determining $E(\mathbf{n}_p')$ exactly in the Cartesian space as

$$E(\mathbf{n}_p') = \frac{1}{2}\sum_{i=1}^{N} m_i\mathbf{v}_{i,p}^{nr}(\mathbf{v}_{i,p}^{nr})^T + V(\mathbf{r}_{1,p}, \mathbf{r}_{2,p}, ..., \mathbf{r}_{N,p})$$
$$- V(\mathbf{r}_1^{eq}, \mathbf{r}_2^{eq}, ..., \mathbf{r}_N^{eq}) \tag{19}$$

where $\mathbf{v}_{i,p}^{nr}$ is the velocity of the pth product corresponding to zero angular momentum as defined in eq 7 and V is the potential energy of the N-atomic product. Approach (2) uses eqs 19 and 18 for $E(\mathbf{n}_p')$ and $E(\mathbf{n})$, respectively. As we showed for the $(H_2O)_2 \rightarrow 2H_2O(n_1n_2n_3)$ [ref 50] and $Cl + CH_4 \rightarrow H + CH_3Cl(n_1n_2n_3n_4n_5n_6)$ [ref 46] reactions, even if approach (1) performs much better than HB, approach (1) provides small populations for some of the energetically closed states due to the failure of the normal-mode analysis, whereas approach (2) gives physically correct results. Thus, approach (2) is recommended instead of approach (1).

(3) We proposed in ref 46 to incorporate the effect of vibrational anharmonicity by using the second-order vibrational perturbation theory (VPT2) to calculate $E(\mathbf{n})$ as

$$E(\mathbf{n}) = \sum_{k=1}^{3N-6} \omega_k\left(n_k + \frac{1}{2}\right) + \sum_{k\geq l}^{3N-6} \chi_{k,l}\left(n_k + \frac{1}{2}\right)\left(n_l + \frac{1}{2}\right) \tag{20}$$

where $\chi_{k,l}$ are the anharmonicity constants, which can be nowadays obtained routinely by ab initio program packages for large polyatomic molecules. Approach (3) calculates the weight from the anharmonic energies $E(\mathbf{n}'_p)$ and $E(\mathbf{n})$ utilizing eqs 19 and 20, respectively. Approaches (2) and (3) were found to give similar results for the Cl + CH_4 → H + CH_3Cl reaction.[46] Recently, this approach was applied to OH* + H_2 → H + H_2O,[66] where the "exact" nearly complete line list with assignments is available for H_2O;[67] thus, the exact quantum vibrational energies were used for $E(\mathbf{n})$. In this case, approach (3) was found to give slightly better results than the harmonic energy-based approach (2). For H_2O one can allow using the traditional mode-based GB approach, where the weight of H_2O is a product of three Gaussians. Reference 66 shows that 1GB gives better results than the computationally more expensive GB. The reason is that 1GB via approaches (2) and (3) solves both the rounding issue and the normal-mode analysis breakdown problem, whereas GB solves the former issue only.

C. Reduced-Dimensional Quantum Dynamics. There are several reduced-dimensional models developed for quantum dynamics studies of the X + YCZ_3 → XY + CZ_3 type reactions. The simplest model is the 2-dimensional (2D) rotating line model (RLM),[68] in which the X and Y atoms and the center of mass of CZ_3 can move along the C_3 axis of the system. The geometry of CZ_3 is usually fixed at the saddle-point value. Clary and co-workers frequently use a 2D model to study polyatomic reactions.[69] In their 2D model the active coordinates are also the breaking and forming bond lengths, but the constrained coordinates are not fixed. In their studies the nonactive coordinates are relaxed and the harmonic zero-point energy of each constrained mode is added to the effective potential.

The RLM model was improved by Yu and Nyman introducing the 3D rotating line umbrella (RLU)[70] and the 4D rotating bond umbrella (RBU)[71] models. In the RLU model the umbrella mode of CZ_3 is also explicitly treated beside the XY and YC stretching modes, but the C_{3v} symmetry of the whole system is still maintained. In the RBU model the reactant bending motion is added to the active coordinates; thus, the C_{3v} symmetry is only maintained for CZ_3, and the collinear X−Y−C arrangement is not forced. The Hamiltonians in the RLU and RBU models were derived in hyperspherical coordinates.

The semirigid vibrating rotor target (SVRT) model is a general 4D model for atom + polyatom reactions, where the polyatomic reactant is treated as a semirigid vibrating rotor.[72] For the X + YCZ_3 reactions the four active coordinates are r, R, θ, and χ, where r is the distance between Y and CZ_3, R is distance between X and YCZ_3, θ denotes the angle between the $\mathbf{r}$ and $\mathbf{R}$ vectors, and χ is the rotational angle of YCZ_3 about the YC axis. Later, a generalized SVRT (GSVRT)[73] model was proposed in which additional vibrational modes of the polyatomic reactant can be treated explicitly. In practice, a 5D GSVRT model was applied to the X + YCZ_3 reactions, where the umbrella motion of CZ_3 was added to the active coordinates.[74]

A 6D model was proposed by Wang and Bowman,[75] in which the X + YCZ_3 reaction is treated as an atom + pseudotriatom system, where Z_3 is replaced by the pseudoatom. The Hamiltonian is written in Jacobi coordinates, where the distance between C and the center of mass of Z_3 describes the umbrella motion of CZ_3.

Palma and Clary developed an 8D model for the X + YCZ_3 system,[76] where the only restriction is that the C_{3v} symmetry of CZ_3 is maintained. In this 8D model, both the umbrella and the symmetric stretching modes of the CZ_3 unit are active. One can also define a 7D model by fixing the CZ bond length, which is often done in applications. Zhang and co-workers reported many state-of-the-art quantum studies on the X + methane reactions using this 7D model.[77−79] Recently, Liu et al.[80] proposed a useful simplification to the Palma−Clary model by assuming that CZ_3 can rotate freely with respect to its C_3 axis, thereby reducing the dimensionality from 8D to 7D or from 7D to 6D if the CZ bond length is fixed.

III. APPLICATIONS TO THE X + METHANE [X = F, O, Cl, Br] REACTIONS

A. Potential Energy Surfaces. *1. Ab Initio Energy Points.* The first step in the PES development is the selection of the structures, which cover the configuration space of chemical importance and the computation of the ab initio energies at the selected geometries. The configurations are usually sampled by running direct dynamics simulations using low-level methods and small basis sets. Furthermore, we add geometries obtained from randomly displaced coordinates of known stationary points (minima and saddle points). In order to ensure the correct asymptotic behaviors we compute separate fragment data for each reaction channel of chemical importance. These so-called fragment data are obtained by adding the energies of the fragments whose coordinates are placed far from each other, e.g., 8 to 20 bohr, depending on the strength of the long-range interactions.

The accuracy of the energy points determines the quality of the PES; therefore, it is important to choose an ab initio level of theory that gives reasonably accurate energies with affordable computational time. In 2014, Czakó and co-workers[81] reported a detailed calibration study of various standard, explicitly correlated F12, and composite ab initio methods with different correlation consistent basis sets for high-dimensional PES developments. For the F, Cl, O(^{3}P), and Br + CH_4 reactions, we used composite methods, where the energies are obtained as[82−85]

$$E[\text{A/small}] + E[\text{B/large}] - E[\text{B/small}] \tag{21}$$

In eq 21, A and B denote an expensive and a less expensive method, respectively, and small and large denote the size of the basis sets. As shown in previous studies,[82,61,84,85] eq 21 provides A/large-quality results without performing the very time-consuming A/large computations. The actual choice of A and B and small and large was made after careful test computations for each system. For F + CH_4, A is UCCSD(T) and B is UMP2, and small and large bases are aug-cc-pVDZ and aug-cc-pVTZ, respectively.[82] For O(^{3}P) + CH_4, we used an even larger basis of aug-cc-pVQZ.[84] In the case of Cl + CH_4, B/large was all-electron (AE) UMP2/aug-cc-pCVTZ, whereas B/small was frozen-core UMP2/aug-cc-pVDZ, thereby accounting for the core correlation effect.[83] For Br + CH_4, the correlation of the core electrons and the scalar relativistic effects are especially important; thus, we used AE-UCCSD(T) and AE-UMP2 for A and B, respectively, and aug-cc-pwCVDZ-PP and aug-cc-pwCVTZ-PP relativistic effective core potential basis sets.[85]

The spin−orbit (SO) splittings, ε, between the ground ($^2P_{3/2}$) and excited ($^2P_{1/2}$) SO states of the F, Cl, and Br atoms are 404, 882, and 3685 cm^{-1}, respectively.[86] Therefore, for the entrance channel of the halogen + methane reactions, the SO coupling plays an important role since it lowers the reactant asymptote by

$\varepsilon/3$, thus effectively increasing the barrier height, and has a significant effect on the entrance channel van der Waals (vdW) well. For F + CH_4 we developed a SO correction surface for the entrance channel using a 3-dimensional rigid methane model.[87] This SO correction surface can be combined with the full-dimensional non-SO PES of the F + CH_4 reaction resulting in a full-dimensional PES for the SO ground-state reaction. Recently, Manthe and co-workers[88] developed SO coupled diabatic local PESs for all the three electronic states of the entrance channel of the F + CH_4 reaction. For the Cl and Br + CH_4 reactions, we followed another strategy in order to account for the SO effect.[83,85] First, we selected the entrance-channel geometries from the total set of configurations based on the following geometrical conditions:

$$r(\mathrm{C{-}X}) > R_{\mathrm{CX}} \quad \min[r(\mathrm{H{-}X})] > R_{\mathrm{HX}} \quad \max[r(\mathrm{C{-}H})] < R_{\mathrm{CH}} \tag{22}$$

where the R_{CX}, R_{HX}, and R_{CH} parameters were chosen to be 2.4/2.0, 1.8/1.5, and 1.3/1.4 Å, for the X + CH_4 [X = Cl, Br] reactions.[61,85] Second, we performed SO computations at the MRCI+Q level using the interacting states approach[89] at the above selected configurations, and the differences between the SO and non-SO ground state electronic energies were added to the composite non-SO energies. The MRCI+Q computations utilized a minimal active space of 5 electrons in the 3 spatial 3p/4p orbitals corresponding to the Cl/Br atom. We performed frozen-core computations with aug-cc-pVTZ and all-electron computations with aug-cc-pwCVDZ-PP for Cl and Br + CH_4, respectively, which provided SO splittings of 798 and 3747 cm^{-1}, whereas the corresponding experimental values are 882 and 3685 cm^{-1}.

2. Fitting the ab Initio Energies. For the X + CH_4 [X = F, $O(^3P)$, Cl, Br] reactions, the initial data set included 10 000–15 000 configurations in the complex region (XCH_4) as well as roughly 2000, 2000, 2000, and 1000 data points for the fragment channels X + CH_4, HX + CH_3, H_2 + CH_2X, and H + CH_3X, respectively. In some cases, e.g., Cl + CH_4,[61] we applied an energy cutoff, e.g., 50 000 cm^{-1}, and all the configurations that had energy larger than the cutoff parameter were excluded from the datatset. As described in section II, the PESs were represented by permutationally invariant polynomial expansions in variables $y_{ij} = \exp(-r_{ij}/a)$, where a was fixed at 2 bohr. We included all terms up to total degree six and 3262 coefficients (3250 + 12 for the short-term repulsion) were determined by a weighted linear least-squares fit using a weight function of $E_0/(E + E_0)$, where E_0 = 11 000 cm^{-1} and E is the actual potential energy relative to the global minimum. Note that without the use of permutational symmetry the number of coefficients would have been 54 264 instead of 3250. The root-mean-square (rms) fitting error is usually below 100 cm^{-1} (0.3 kcal/mol) for the chemically most important energy interval of (0, 11 000) cm^{-1}. For the Cl and Br + CH_4 reactions, we fit both the non-SO and SO-corrected data points; thus, PESs were obtained for the non-SO and SO ground electronic states of the X + CH_4 [X = Cl, Br] reactions.[61,85]

3. Properties of the Potential Energy Surfaces. Schematics of the PESs of the X + CH_4 [X = F, $O(^3P)$, Cl, Br] reactions are shown in Figure 1. As seen, there are many similarities as well as differences between the shapes of the PESs. All the reactions have a shallow vdW well in the entrance channel, a first-order saddle point separating the reactants from the products, and a relatively deep CH_3···HX complex in the exit channel. The F + CH_4 reaction is highly exothermic, the $O(^3P)$ and Cl + CH_4 reactions are slightly endothermic, and the Br + CH_4 reaction is highly endothermic. As the Hammond postulate[90] predicts, F + CH_4 is an early barrier reaction (the saddle point has a reactant-like structure), $O(^3P)$ + CH_4 is a central (or late) barrier reaction, and Cl and Br + CH_4 are late-barrier reactions.

In a correct relativistic description, the ground electronic state (^2P) of a halogen atom splits into a 4-fold degenerate SO ground state ($^2P_{3/2}$) and a 2-fold degenerate SO excited state ($^2P_{1/2}$). As mentioned earlier, the energy differences between the $^2P_{3/2}$ and $^2P_{1/2}$ SO states of the F, Cl, and Br atoms are 404, 882, and 3685 cm^{-1}, respectively. When the halogen atom approaches methane, the 4-fold degenerate state splits into two doubly degenerate SO states, and only the SO ground state correlates with electronically ground-state products. Thus, three doubly degenerate SO states are involved in the dynamics of the halogen + methane reactions, but only the ground SO state is reactive within the Born–Oppenheimer (BO) approximation. However, there is evidence for nonadiabatic dynamics. Early studies showed for the prototypical F + H_2 reaction that $F^*(^2P_{1/2})$ can react, though the reactivity of $F(^2P_{3/2})$ is at least 10 times larger.[91] In 2007, evidence was found for significant reactivity of $F^*(^2P_{1/2})$ with D_2 at very low collision energies (<0.5 kcal/mol), e.g., at 0.25 kcal/mol $F^*(^2P_{1/2})$ is ∼1.6 times more reactive than $F(^2P_{3/2})$.[92] For the Cl + CH_2D_2 and Cl + CH_4 reactions, 4–8% relative reactivity of $Cl^*(^2P_{1/2})$ was observed experimentally by Liu and co-workers,[93,94] in good agreement with the 2D quantum dynamics study of Clary and co-workers.[95]

Potential energy curves for the entrance channel of the Cl + CH_4 reaction showing the non-SO and SO states are shown in Figure 2. As seen, there is a shallow vdW well in the entrance channel, whose depth depends on the orientation of the reactants.[83] For the H_3CH···Cl arrangement, the well is about 100 cm^{-1} deep, whereas a significantly deeper depth of about 300 cm^{-1} corresponds to the HCH_3···Cl structure on the non-SO PES. These data were benchmarked by systematic all-electron CCSD(T)/aug-cc-pCVnZ [n = D, T, Q] computations with and without counterpoise corrections.[61] The SO coupling has negligible effect on the depth of the former, whereas it reduces the depth of the latter. Nevertheless, the HCH_3···Cl remains the deeper minimum with $D_e \cong 200$ cm^{-1} on the SO ground-state surface, as well. As also shown in Figure 2, the one-dimensional cuts of the analytical non-SO and SO PESs are in good agreement with the benchmark ab initio entrance-channel potentials. For the other halogen + methane reactions the entrance-channel potentials have similar characteristics as that of Cl + CH_4; the only main difference is in the magnitude of the energy differences between the various electronic states, due to the increasing SO splitting from F to Br. The picture is different for the $O(^3P)$ + CH_4 reaction since $O(^3P)$ splits into a 5-fold degenerate SO ground state ($^3P_2$) and 3-fold degenerate ($^3P_1$) and nondegenerate ($^3P_0$) excited SO states. The energies of $O(^3P_1)$ and $O(^3P_0)$ are 158 and 227 cm^{-1} relative to $O(^3P_2)$.[86] Thus, the non-SO $O(^3P)$ state is above the SO ground state by only 78 cm^{-1}. When the O atom approaches methane the degenerate SO states split and the 5 components of $^3P_2$ and one component of $^3P_1$ correlate with electronically ground-state products, whereas two components of $^3P_1$ and $^3P_0$ correlate with excited products. So far, SO surfaces have not been developed for the $O(^3P)$ + CH_4 reaction. Nevertheless, the dynamics can be well described on the non-SO ground electronic state since the magnitude of the SO splittings is significantly smaller than that in the halogen + CH_4 reactions, especially considering the Cl and Br + CH_4 systems.

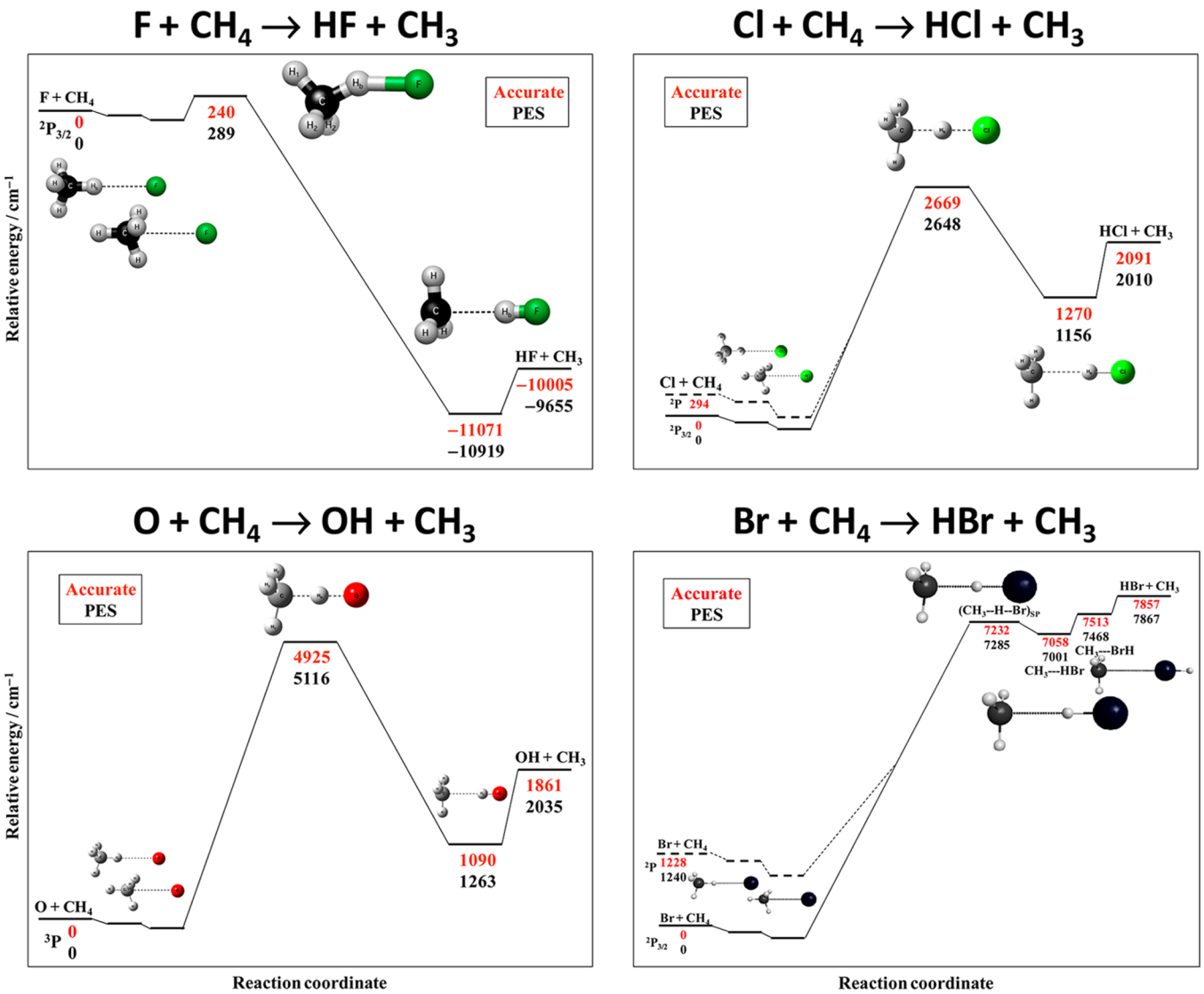

Figure 1. Schematics of the potential energy surfaces of the F, O(^{3}P), Cl, and Br + CH_4 reactions showing the structures and energies (without ZPE) of the stationary points. The benchmark energies (upper red numbers) are obtained by the focal-point analysis approach (see more details in Table 1 and in refs 82−85.

In 2011 Cheng et al.[96] probed the entrance channels of the X + CH_4 [X = F, Cl, Br, I] reactions via photoelectron spectroscopy of the corresponding X^-−CH_4 anion complex. Furthermore, for the F and Cl + CH_4 systems, Neumark and co-workers[97−99] reported slow electron velocity-map imaging (SEVI) spectra. For the late-barrier Cl, Br, and I + CH_4 reactions, the equilibrium structure of X^-−CH_4 (single H-bonded structure with C_{3v} point-group symmetry) overlaps with the entrance-channel vdW region of the PES; thus, the doublet splittings observed in the spectra of the complexes are close to the corresponding isolated atomic SO splittings.[96] However, for the early barrier F + CH_4 reaction a much larger splitting (∼1310 cm^{-1}) was observed in the spectrum of F^-−CH_4 than the SO splitting (404 cm^{-1}) of the F atom (see Figure 3).[96] As shown in Figure 3, ab initio computations of the SO splitting as a function of the C−F distance of the H_3CH−F system gave a splitting close to the experimental value at a C−F separation that corresponds to the equilibrium distance in F^-−CH_4. Therefore, our interpretation was that the second peak in the spectrum corresponds to a transition to an excited electronic state of the neutral system.[96] Note that the SO ground and excited states of the neutral system converge to the ground and excited non-SO electronic states, respectively, when the C−F separation approaches the equilibrium distance of the anion complex. Therefore, the doublet splitting of the complex can be explained considering simply the non-SO electronic states. Our interpretation was confirmed in 2013 by Manthe and co-workers[88] who carried out full-dimensional MCTDH simulations of the photodetachment spectrum of F^-−CH_4 using ab initio PESs developed for the entrance channel of the F + CH_4 reaction and the F^-−CH_4 PES of ref 100. The simulations showed that the major contribution to the second peak comes from the excited electron state and the bending excitation of the CH_4 unit, which has energy comparable to the observed splitting of ∼1310 cm^{-1}, has a minor effect on the second peak. A very recent joint experimental−theoretical study found resonance features in the SEVI spectra of F^-−CH_4 and F^-−CD_4.[99] The MCTDH simulations showed that periodic hindered rotations of CH_4 relative to F and CH_4···F type stretching motions are responsible for the fine structure of the spectra.

As described earlier, the SO ground-state PESs of the halogen + CH_4 reactions are developed by using the SO − non-SO energy

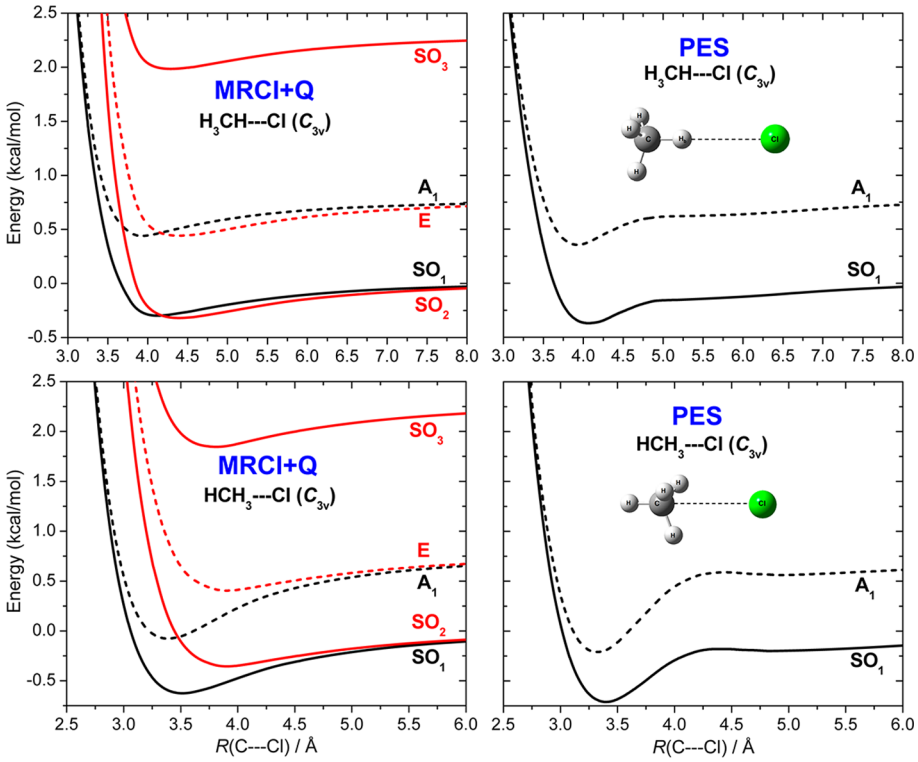

Figure 2. Potential energy curves for the entrance channel of the Cl + CH_4 reaction as a function of the C···Cl distance along the C_3 axis with fixed CH_4(eq) geometry. The left panels show the direct ab initio results obtained at the MRCI+Q/aug-cc-pVTZ level of theory, whereas the right panels show the one-dimensional cuts of the non-SO and SO ground-state PESs. A_1 and E denote the non-SO ground and excited electronic states, respectively, and SO_1, SO_2, and SO_3 are the three SO states. Adapted from ref 83.

differences obtained from MRCI+Q computations as additive corrections to the non-SO PES. Figure 4 shows the SO correction curves for the entrance channels of the Cl and Br + CH_4 reactions. The shape of the curves is similar for both systems; the difference is in the magnitude of the SO effect. For Cl and Br + CH_4, the reactant asymptotes are lowered by roughly 300 and 1200 cm^{-1}, respectively. The absolute SO correction decreases as the halogen atom approaches CH_4 and tends to vanish at around C−X distance of 2 Å. Figure 4 shows that the SO correction depends on the orientation of the reactant, and the effect is larger at HCH_3···X structures than at H_3CH···X geometries. For Br + CH_4, Figure 4 also shows that the energy differences between the SO and non-SO analytical PESs are in good agreement with the direct ab initio MRCI+Q data.[85]

The structures of the saddle points, CH_3···HX complexes, reactants, and products, as well as relative energies such as barrier heights, dissociation energies of CH_3···HX, and reaction energies for X + CH_4 [X = F, O(^{3}P), Cl, Br] are collected in Table 1. The PES values are compared to benchmark ab initio data determined by the focal-point analysis (FPA)[101,102] approach. The FPA uses accurate geometries obtained usually at the AE-UCCSD(T)/aug-cc-pCV*n*Z [*n* = T or Q] level of theory. The relative energies are benchmarked by single-point computations at the above-defined high-level structures considering the following: (a) extrapolation[103,104] to the complete basis set (CBS) limit using either aug-cc-pCV*n*Z [*n* = Q, 5] or aug-cc-pV*n*Z [*n* = 5, 6] basis sets, (b) post-CCSD(T) correlation effects by performing CCSDT and CCSDT(Q) computations, (c) core-correlation effects by either extrapolating to the CBS limit using AE-UCCSD(T)/aug-cc-pCV*n*Z [*n* = Q, 5] energies or using the difference between the AE and frozen-core UCCSD(T)/aug-cc-pCVQZ energies as an additive correction to the frozen-core CBS limit, (d) scalar relativistic effects obtained at the Douglas−Kroll[105] AE-UCCSD(T)/aug-cc-pCVQZ level of theory, and (e) SO effects.

Among the halogen + methane reactions, F + CH_4 has the unique feature that the saddle-point geometry is slightly bent with a C−H−F angle of about 150°.[82] Note that both MP2 and CCSD found a collinear C_{3v} saddle-point structure; the CCSD(T) method is needed to get the bent C_s structure.[82] It is also important to note that the saddle-point structure is very fluxional and that the energy difference between the collinear and bent structures is only a few cm^{-1}. The saddle-point structure of O(^{3}P) + CH_4 is also slightly bent due to the interaction between two electronic states, ^{3}A′ and ^{3}A″ considering C_s symmetry, which are degenerate at C_{3v} structures. AE-CCSD(T)/aug-cc-pCVQZ computation gives a C−H−O angle of 179.3° at the saddle point and an energy below the C_{3v} structure by only ∼1 cm^{-1}.[84] The saddle points of the Cl and Br + CH_4 reactions have exactly collinear structures with C_{3v} point-group symmetry. As mentioned earlier, the F, O(^{3}P), Cl, and Br + CH_4 reactions are early-, central-, late-, and late-barrier reactions, respectively. Indeed, at the saddle point, the C−H_b distances, where H_b is the abstracted H atom, increase as 1.111, 1.288, 1.397, and 1.674 Å, for F, O, Cl, and Br + CH_4, respectively, i.e., stretched by 0.024, 0.201, 0.310, and 0.587 Å, in order, relative to the CH bond length in CH_4. The H_b−X distances are stretched at the saddle point by 0.704, 0.243, 0.169, and 0.073 Å, for X = F, O, Cl, and Br, respectively, relative to the bond length of the isolated HX molecule. On the basis of the above structural parameters, it is clear that the saddle point of F + CH_4 is reactant-like, whereas the saddle points of Cl and Br + CH_4 are product-like. In the case of O(^{3}P) + CH_4, both CH_b and H_bO distances are similarly stretched; thus, O(^{3}P) + CH_4 can be called a central-barrier

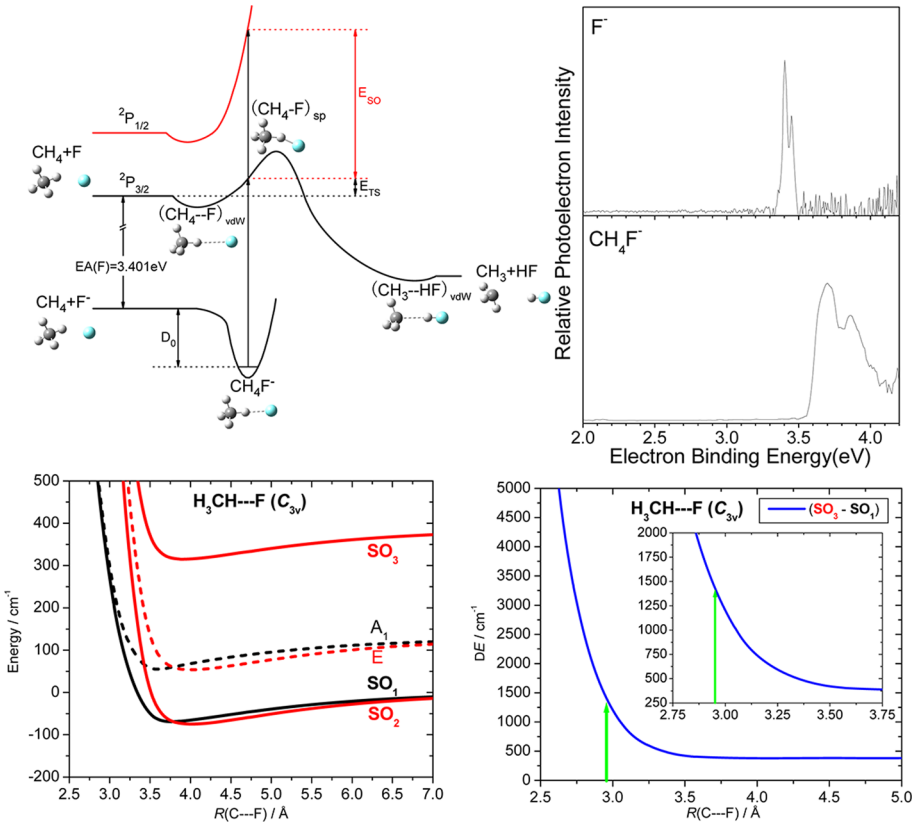

Figure 3. Diagram of the potentials of the F^--CH_4 and $F-CH_4$ systems and the measured photoelectron spectra of F^- and F^--CH_4 taken with 266 nm photons (upper panels). Potential energy curves (lower left panel) and spin−orbit splittings (lower right panel) of $CH_4\cdots F$ as a function of the C···F distance along the C_3 axis with fixed CH_4(eq) geometry and C−H···F linear bond arrangement computed at the MRCI+Q/aug-cc-pVTZ level of theory. See Figure 2 for the notations. Green arrows indicate the C···F equilibrium distance in the anion complex and the corresponding vertical splitting of the neutral system. Adapted from ref 96.

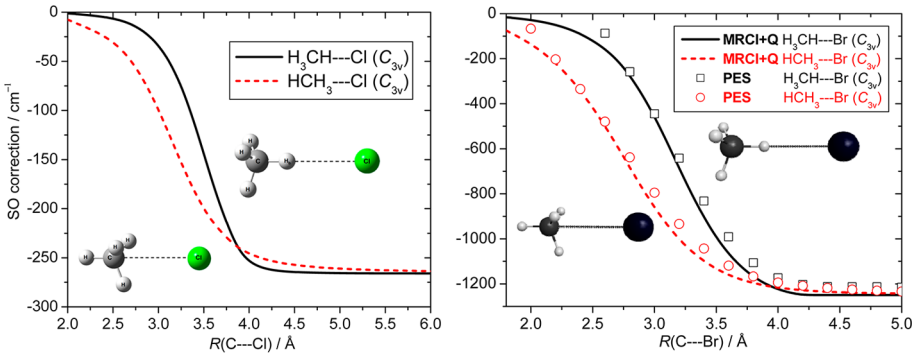

Figure 4. Spin−orbit correction curves for the entrance channel of the Cl + CH_4 (left) and Br + CH_4 (right) reactions as a function of the C···X distance along the C_3 axis keeping CH_4 at equilibrium with $H_3CH\cdots X$ and $HCH_3\cdots X$ orientations [X = Cl, Br]. The SO correction is defined as difference between the SO and non-SO ground-state electronic energies. The curves were obtained by frozen-core MRCI+Q/aug-cc-pVTZ and all-electron ECP-MRCI+Q/aug-cc-pwCVDZ-PP levels of theory for Cl and Br + CH_4, respectively. For Br + CH_4, the PES values, i.e., differences between the SO and non-SO PESs, are also shown for comparison. Adapted from refs 61 and 85.

reaction, though this category is not well-defined, therefore, in the literature $O(^3P)$ + CH_4 is sometimes called as early- or late-barrier reaction.

In the product channel of all the X + CH_4 [X = F, $O(^3P)$, Cl, Br] reactions there is a relatively stable $CH_3\cdots HX$ complex with C_{3v} point-group symmetry. As Table 1 shows, the structures of the four $CH_3\cdots H_bX$ complexes are similar. The CH_b distances are 2.1−2.3 Å, the HCH_b angles are ∼93°, and the CH and H_bX distances agree with the corresponding CH_3 and HX bond lengths within 0.001−0.002 and 0.005−0.013 Å, respectively. The benchmark dissociation energies (D_e) of $CH_3\cdots HX$ are 1066, 771, 821, and 799 cm^{-1} for X = F, O, Cl, and Br, respectively.

The highly exothermic, ΔE_e = −10 137/−10 005 cm^{-1}, $F(^2P/^2P_{3/2})$ + CH_4 reaction has a low classical barrier height of 117/240 cm^{-1}, whereas the $O(^3P)$, $Cl(^2P/^2P_{3/2})$, and $Br(^2P/^2P_{3/2})$ + CH_4 reactions are endothermic, ΔE_e = 1861, 1797/2091, and 6629/7857 cm^{-1}, respectively, with corresponding classical barrier heights of 4925, 2375/2669, and 6004/7232 cm^{-1}. Since the SO correction lowers the reactant

Table 1. Properties of the Potential Energy Surfaces of the X + CH_4 → HX + CH_3 [X = F, O(^{3}P), Cl, Br] Reactions Showing the Structures (Å and Degrees) and Relative Energies (cm^{-1}) of the Stationary Points

	F + CH_4[a]		O(^{3}P) + CH_4[b]		Cl + CH_4[c]		Br + CH_4[d]	
	PES	accurate	PES	accurate	PES	accurate	PES	accurate
Saddle Point (H_3C-H_b-X)								
r(CH)	1.091/1.089	1.088/1.087	1.086/1.086	1.083/1.083	1.083	1.083	1.081	1.081
r(CH_b)	1.105	1.111	1.305	1.288	1.403	1.397	1.710	1.674
r(H_bX)	1.656	1.621	1.198	1.213	1.437	1.443	1.484	1.486
α(HCH_b)	106.5/108.6	107.2/108.3	103.7/103.7	104.1/103.6	101.0	101.1	96.9	97.4
Classical Barrier Height								
non-SO	167	117	5116	4925	2384	2375	6039	6004
SO	289	240			2648	2669	7285	7232
$CH_3\cdots H_bX$ Complex								
r(CH)	1.083	1.078	1.081	1.078	1.080	1.078	1.080	1.079
r(CH_b)	2.208	2.142	2.337	2.269	2.274	2.236	2.210	2.184
r(H_bX)	0.927	0.925	0.974	0.975	1.282	1.284	1.421	1.426
α(HCH_b)	93.9	93.1	93.0	92.6	92.8	92.6	92.5	93.0
D_e	1264	1066	772	771	854	821	867	799
Reactants and Products (CH_4, CH_3, HX)								
r_{CH}(CH_4)	1.091	1.087	1.089	1.087	1.089	1.087	1.089	1.087
r_{CH}(CH_3)	1.081	1.077	1.079	1.077	1.079	1.077	1.078	1.077
r(HX)	0.922	0.917	0.973	0.970	1.276	1.274	1.412	1.413
Classical Reaction Energy								
non-SO	−9784	−10137	2035	1861	1751	1797	6637	6629
SO	−9655	−10005			2010	2091	7867	7857

[a]The PES structures and non-SO energies correspond to the PES of ref 82, whereas the SO energies correspond to the hybrid SO-corrected PES of ref 87. The accurate structures are obtained at all-electron (AE) UCCSD(T)/aug-cc-pCVTZ (saddle point) and AE-UCCSD(T)/aug-cc-pCVQZ (all the other species). The accurate energies are obtained from the focal-point analysis (FPA) of ref 82. The saddle point has a bent C_s structure with α(CH_bF) = 144.4° (PES) and 152.3° (accurate); therefore, two different r(CH) and α(HCH_b) exist as shown in the table. [b]The PES structures and energies correspond to the PES of ref 84. The accurate structures are obtained at AE-UCCSD(T)/aug-cc-pCVQZ, and the relative energies are AE-CCSDT(Q)/CBS quality FPA results from ref 84. The saddle point is slightly bent (C_s symmetry and ^{3}A″ electronic state) with α(CH_bO) = 179.3° (accurate); therefore, two different r(CH) and α(HCH_b) exist as shown in the table. [c]The PES results correspond to the non-SO and SO PESs of ref 83, showing the SO PES structures. The accurate structures are obtained at AE-UCCSD(T)/aug-cc-pCVTZ (saddle point) and AE-UCCSD(T)/aug-cc-pCVQZ (all the other species). The accurate energies are relativistic AE-CCSDT(Q)/CBS quality FPA results from ref 83. [d]The PES results correspond to the non-SO and SO PESs of ref 85, showing the SO PES structures. The accurate structures are obtained at AE-ECP-UCCSD(T)/aug-cc-pwCVTZ-PP (saddle point and $CH_3\cdots$HBr), AE-UCCSD(T)/aug-cc-pCVQZ (CH_4 and CH_3), and AE-ECP-UCCSD(T)/aug-cc-pwCVQZ-PP (HBr), and the relative energies are relativistic AE-CCSDT(Q)/CBS quality FPA results from ref 85.

asymptotes, the barrier heights and reaction energies are effectively increased as shown above for the halogen + CH_4 reactions. This SO energy shift is larger from F to Br. However, considering the relative effect on the barrier heights, the SO effect is the most significant for the low-barrier F + CH_4 reaction, where the SO correction doubles the classical barrier height. Note that for the late-barrier Cl and Br + CH_4 reactions the SO correction quenches at the saddle point; thus, the SO effect on the barrier height comes from the SO shift of the reactant asymptote. However, for the early barrier F + CH_4 reaction, a small SO correction of about −8 cm^{-1} remains at the saddle point. It is also interesting to note that the saddle point of the Br + CH_4 reaction is below the product asymptote by 625 cm^{-1}; thus, the backward reaction, HBr + CH_3, has a negative barrier.[85]

For the Cl($^2P_{3/2}$) and Br($^2P_{3/2}$) + CH_4 reactions the analytical SO PESs[61,85] give barrier heights of 2648(2669) and 7285(7232) cm^{-1}, respectively, and reaction energies of 2010(2091) and 7867(7857) cm^{-1}, respectively, in excellent agreement with the benchmark FPA values shown in parentheses. It is remarkable (and fortuitous) that the PESs reproduce the relativistic AE-CCSDT(Q)/CBS-quality FPA data with an average deviation of only 0.1 kcal/mol. For the F($^2P_{3/2}$) and O(^{3}P) + CH_4 reactions, the PES(FPA) barrier heights are 289(240) and 5116(4925) cm^{-1}, respectively, and the reaction energies are −9655(−10005) and 2035(1861) cm^{-1}, respectively. Here, the average error is about 0.5 kcal/mol, which is still quite good, since chemical accuracy is usually defined as an accuracy of 1 kcal/mol. The largest error is found for the reaction energy of F($^2P_{3/2}$) + CH_4. Nevertheless, the exothermicity of the CCSD(T)/aug-cc-pVTZ-quality SO PES, −9655 cm^{-1}, agrees well with the direct ab initio CCSD(T)/aug-cc-pVTZ result (+ SO correction) of −9639 cm^{-1}. The difference of about 1 kcal/mol between the CCSD(T)/aug-cc-pVTZ and FPA reaction energy data mainly comes from the basis set incompleteness error of aug-cc-pVTZ. (Note that ref 81 shows that CCSD(T)/aug-cc-pVTZ has an average accuracy of 1 kcal/mol for systems involving first and second row elements.) Finally, we emphasize that electron correlation plays an important role in the accurate computation of the barrier height of the F + CH_4 reaction since the ROHF, RMP2, UCCSD, UCCSD(T), UCCSDT, and UCCSDT(Q) classical CBS non-SO barrier heights are 3292, 1080, 628, 194, 144, and 109 cm^{-1}, respectively.[82] The benchmark SO value of 240 cm^{-1} was obtained as UCCSDT(Q)/CBS + scalar relativistic correction + diagonal BO correction + SO correction = 109 + 3 + 5 + 123 cm^{-1}.

B. Reaction Dynamics Computations. *1. Integral Cross-Sections and Reaction Probabilities.* Reaction probabilities and integral cross-sections (ICSs) for the Cl + CH_4(v = 0) reaction obtained from QCT calculations using the ab initio PES of ref 83 are shown in Figures 5 and 6, respectively. The PES describes

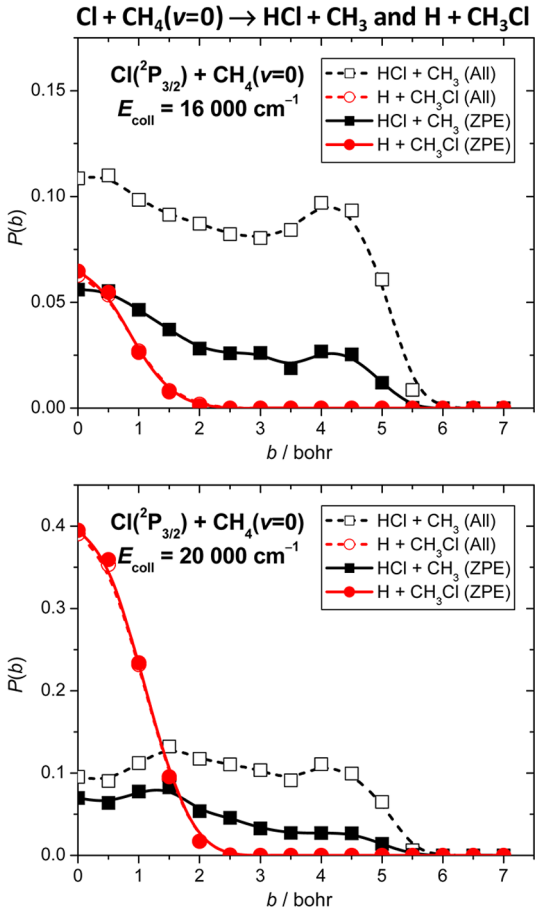

Figure 5. Probabilities of the $Cl(^2P_{3/2}) + CH_4(v = 0) \rightarrow HCl + CH_3$ and $H + CH_3Cl$ reactions as a function of the impact parameter at collision energies of 16 000 and 20 000 cm^{-1}. The probabilities were obtained considering all the trajectories ("All") as well as ZPE constrained trajectories ("ZPE") in which CH_3 or CH_3Cl has at least zero-point vibrational energy. Adapted from ref 61.

both the abstraction ($HCl + CH_3$) and substitution ($H + CH_3Cl$) channels. At low collision energies (E_{coll}) only the abstraction channel is energetically accessible; the substitution channel opens at $E_{coll} \approx 13\,000$ cm^{-1} and then the cross-section of the substitution reaction rapidly increases. At E_{coll} = 18 000 and 20 000 cm^{-1} the H/HCl ratios are 0.09(0.29) and 0.21(0.62), respectively. The ratios in parentheses show the ZPE-constrained QCT results, where trajectories are discarded if CH_3 or CH_3Cl has less vibrational energy than the corresponding ZPE. As seen, the ZPE constraint significantly increases the H/HCl ratio because many CH_3 products violate ZPE, whereas CH_3Cl is usually highly excited. As Figure 5 shows the shape of opacity functions, reaction probability (P) vs impact parameter (b), of the abstraction and substitution channels is quite different. The maximum impact parameters are about 6 and 2 bohr for the abstraction and substitution channels, respectively. The substitution has the highest probability at b = 0, and $P(b)$ decreases rapidly with increasing b. For the abstraction channel, $P(b)$ is nearly constant in the 0−5 bohr impact parameter range and drops quickly between b = 5 and 6 bohr. At small impact parameters the rebound mechanism dominates. For the abstraction reaction the stripping mechanism is also significant causing the larger b_{max} value. In Figure 6 the SO effect on the ICSs is also shown. Since the SO correction effectively increases the barrier height, we can expect smaller ICSs on the SO PES. Indeed, the ICSs are about 2 times larger on the non-SO PES than on the SO PES at a low E_{coll} of about 2000 cm^{-1}, and the SO effect is still about 10−20% in the E_{coll} range of 10 000−20 000 cm^{-1}. These SO effects are not sensitive to the ZPE issue of QCT because the ZPE constraint has virtually the same effect on the non-SO and SO results.

The $Cl + CHD_3$ reaction has become a benchmark system for testing the mode selectivity and the validity of the Polanyi rules for polyatomic reactions. Following the mode-specific experiments performed for Cl + methane (CH_4, CH_3D, etc.) in the groups of Crim and Zare,[14,13] in 2007 Liu and co-workers[18] found that CH stretching excitation is no more efficient than translational energy in promoting the late-barrier $Cl + CHD_3 \rightarrow HCl + CD_3(v = 0)$ reaction, in contradiction to the extended Polanyi rules. Note that the Polanyi rules were designed for atom + diatom reactions; thus, one may expect that these rules cannot be simply extended for polyatomic reactions, where many vibrational degrees of freedom exist. In 2011 we developed a full-dimensional ab initio PES for the Cl + methane reaction and carried out QCT calculations for $Cl + CHD_3(v_k = 0,1) \rightarrow HCl + CD_3$ [k = 1, 3, 5, 6].[83] Figure 7 shows the computed ICSs as a function of E_{coll} and the vibrational enhancement factors as functions of E_{coll} and total energy (E_{coll} + vibrational energy of CHD_3). As seen, the excitation of the bending modes [$\nu_3(a_1)$, $\nu_5(e)$, and $\nu_6(e)$] and especially the CH stretching [$\nu_1(a_1)$] excitation enhance the reactivity. However, these enhancement factors are obtained at the same E_{coll}, which does not correspond to the same total energy of the ground-state and reactant vibrationally excited reactions. As was done by Liu and co-workers,[18] in Figure 7 we also plot the enhancement factors as a function of total energy. As seen, at low energies the vibrational excitation does not promote the reaction, in agreement with experiment. Analysis of representative trajectories showed that at low E_{coll} the vdW well in the entrance channel plays an important role in the dynamics. As mentioned before and seen in Figure 2, the vdW well is deeper at HCH_3···Cl orientations than at H_3CH···Cl; thus, the reactants are steered into a nonreactive orientation especially at low E_{coll} as shown in Figure 7. As E_{coll} increases the effect of the shallow vdW well diminishes and vibrational excitation, especially CH stretching excitation, becomes more efficient than translational energy to activate the reaction.

In 2012, Zhang and co-workers[79] performed 7-dimensional quantum mechanical (QM) wave packet dynamics computations for the $Cl + CHD_3(v_1 = 0,1) \rightarrow HCl + CD_3$ reaction using the Palma−Clary model Hamiltonian[76] and the PES of ref 83. As seen in Figure 8, the QM CH stretching enhancement factors are 3−4 times larger than those obtained from QCT and experiment. Both QM and QCT show that at low E_{coll}, CH stretching excitation is less efficient to promote the reaction than an equivalent amount of translational energy, in qualitative agreement with experiment. The fact that the QM ICS ratios are larger than the corresponding QCT results may be reasonable since QCT may miss some quantum effects, for example, CH stretching excitation energy may leak to other modes prior to the collision, thereby decreasing the vibrational enhancement factors. (Note that it was checked by computing the mode energies as a function of time that this leakage problem is not a serious issue in this reaction.) Even if the QM study is not full-dimensional, the QM ICS ratios are the best theoretical predictions for the enhancement factor at present. When we compare theory and experiment, several details should be considered. First, experiment probed ground-state $CD_3(v = 0)$ only.[18] The theoretical

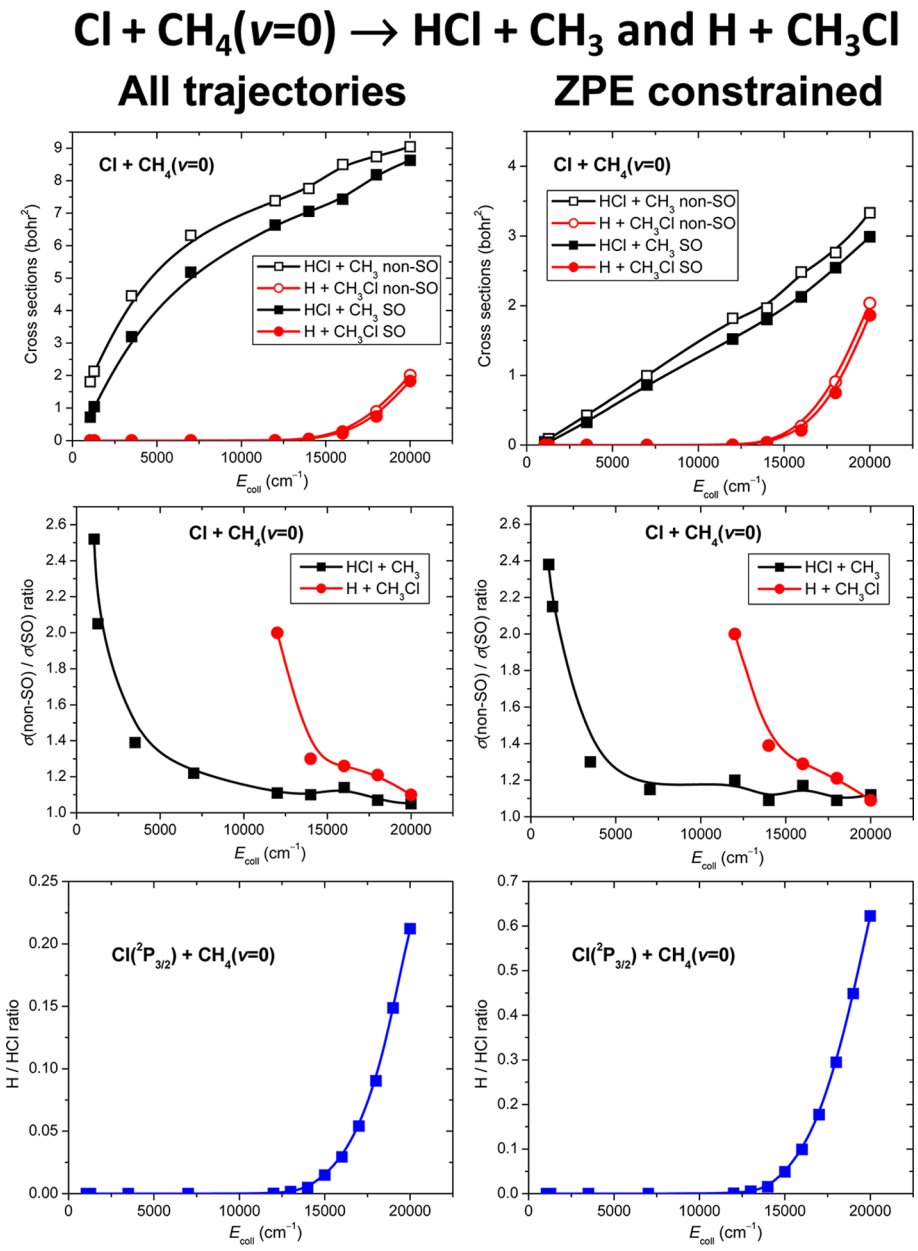

Figure 6. Cross-sections of the Cl + $CH_4(v = 0)$ → HCl + CH_3 and H + CH_3Cl reactions on the SO and non-SO PESs (top); ratios of the non-SO and SO cross-sections (middle); and ratios of the substitution and abstraction channels on the SO PES (bottom) as a function of collision energy. The cross-sections were obtained considering all the trajectories without ZPE constraint (left) as well as ZPE constrained trajectories (right) in which CH_3 or CH_3Cl has at least zero-point vibrational energy. Adapted from ref 61.

study also computed the $CD_3(v = 0)$ resolved ICS ratios as shown in Figure 8 (right B panel), but these QM results overestimate the experimental enhancement factors by a factor of 3−4. Second, experiment probed the low *NK* rotational states of the CD_3 product,[18] whereas the theoretical results correspond to all the *NK* states. This rotational-probe issue inspired an experimental reinvestigation of the Cl + $CHD_3(\nu_1 = 0,1)$ reactions.[106] It turned out that probing all the *NK* states of $CD_3(v = 0)$ increases the vibrational enhancement factors by a factor of 3−4 (Figure 8), thereby resolving the contradiction between QM theory and experiment. However, the story does not end here because the theoretical computations are performed for the $J = 0$ rotational state of the reactants $CHD_3(v = 0)$ and $CHD_3(\nu_1 = 1)$, whereas experiment corresponds to $CHD_3(v = 0, T_{rot} \approx 5-10\ K)$ and $CHD_3(\nu_1 = 1, J = 2, K = 0, \pm 1)$. This reactant rotational probe effect on the vibrational enhancement factor is still an open question and the theoretical and experimental research is ongoing about the initial *JK*-dependence of the reactivity. For the Cl + CH_4 reaction, a 6D QM study[107] found that the reaction probabilities depend on *J* of CH_4, and for Cl + CH_3D, a recent experiment found that higher *J* states are slightly more reactive than low *J* states.[108]

In 2013, Jiang and Guo[109] proposed a sudden vector projection (SVP) model as a more quantitative alternative to the Polanyi rules. The SVP model calculates the overlaps between the normal modes of the reactant and the reaction coordinate vector at the transition state. On the basis of the overlaps, one can predict the efficacy of a specific vibrational mode on the reactivity if the internal energy redistribution prior to the collision is not significant. The limitations of the SVP model were pointed out

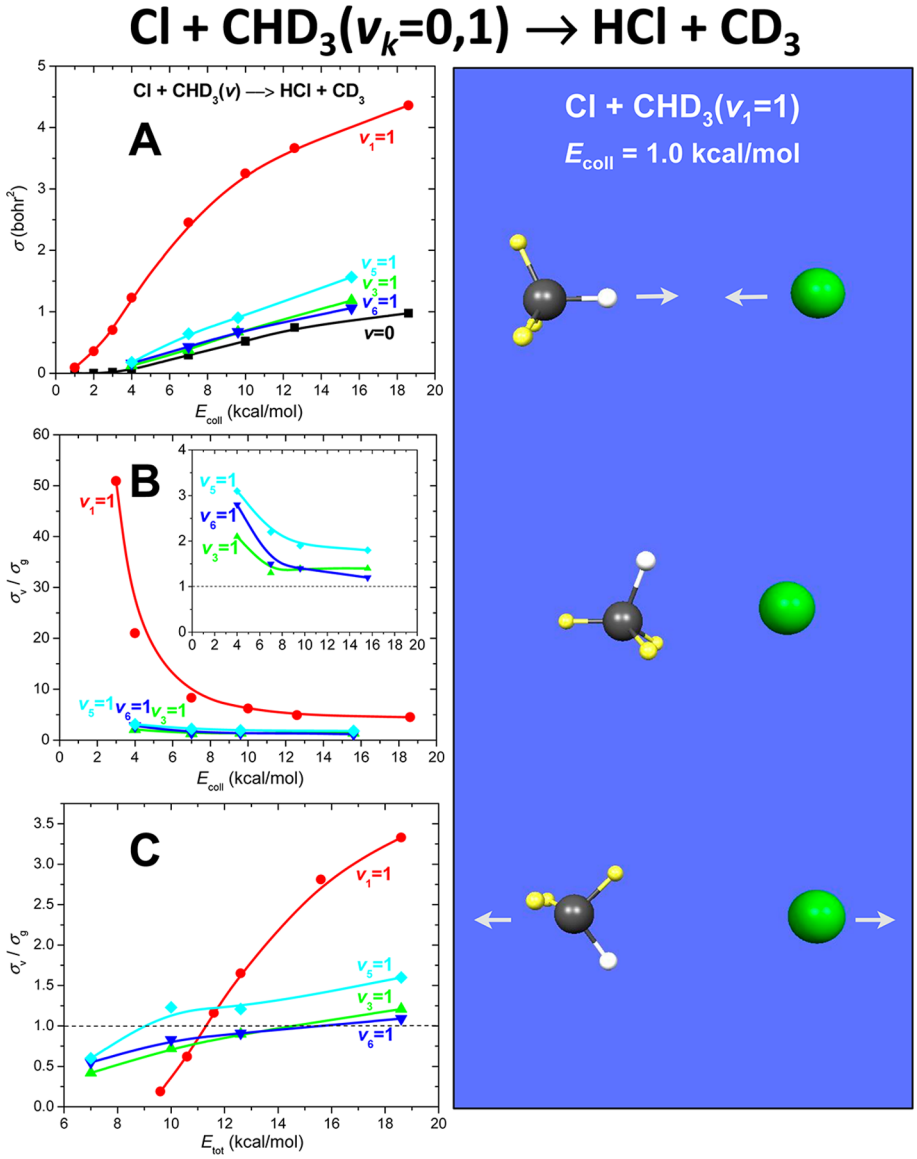

Figure 7. Cross-sections (A) for the Cl + $CHD_3(v_k = 0, 1)$ [k = 1, 3, 5, 6] reactions and their ratios (B) as a function of collision energy (E_{coll}). Presented in panel C are the cross-section ratios at equivalent amounts of total energy ($E_{tot} = E_{coll} + E_v$), where the vibrational energies (E_v) are 0, 8.6, and 3.0 kcal/mol (relative to ZPE) for the ground state and stretch and bend excited reactions, respectively. In the right panel, snapshots of a nonreactive Cl + $CHD_3(v_1 = 1)$ trajectory are shown illustrating the stereodynamics in the van der Waals region causing the unexpected $\sigma_v/\sigma_g < 1$ ratio at E_{tot} = 9.6 kcal/mol as seen in panel C. Adapted from ref 83.

by Jiang and Guo who wrote that "the sudden model is not a panacea and cannot be expected to provide all answers for mode selectivity."[109] For CH stretching and bending excited CHD_3, we showed in refs 45 and 110 that the classical vibrational actions are nearly constant until the reactants collide, which suggests that the SVP model could be useful for X + methane reactions. So far, the model has been applied to atom + diatom systems,[109] X + H_2O reactions,[111] and the methane dissociative chemisorption on Ni(111) surface.[112,113] Application to gas-phase X + methane reactions is a work in progress.

Many dynamical studies were reported for the $O(^3P)$ + CH_4 reaction using full-[114] and reduced-dimensional[115,116] QCT and reduced-dimensional QM[76,77] methods. Most of the studies employed reduced-dimensional ab initio PESs[115] or the full-dimensional semiempirical PES of Espinosa-García and co-workers.[32] The first full-dimensional ab initio PES for this fundamental polyatomic reaction was developed by Czakó and Bowman (CB) in 2012.[84]

For the $O(^3P)$ + $CH_4(v_k = 0,1)$ → OH + CH_3 [k = 1, 2, 3, 4] reactions, full-dimensional QCT and 8-dimensional QM (Palma−Clary model) computations were performed using the ab initio CB PES.[117,62] The comparison of QM, QCT, and experimental[118] ICSs of $O(^3P)$ + $CH_4(v = 0)$ as a function of E_{coll} are shown in Figure 9. As seen, the agreement between QM and QCT as well as theory and experiment is excellent. However, a few important notes have to be mentioned. First, experiment probes $CH_3(v = 0)$ only, whereas the theoretical results correspond to CH_3(all states). As we will discuss later, $CH_3(v = 0)$ is the major product state of the $O(^3P)$ + $CH_4(v = 0)$ reaction. Second, experiment does not measure absolute cross-sections; therefore, the experimental data are scaled by a constant factor to match the QM result at E_{coll} = 14.7 kcal/mol. Third, the QCT results shown in Figure 9 are based on all the trajectories without

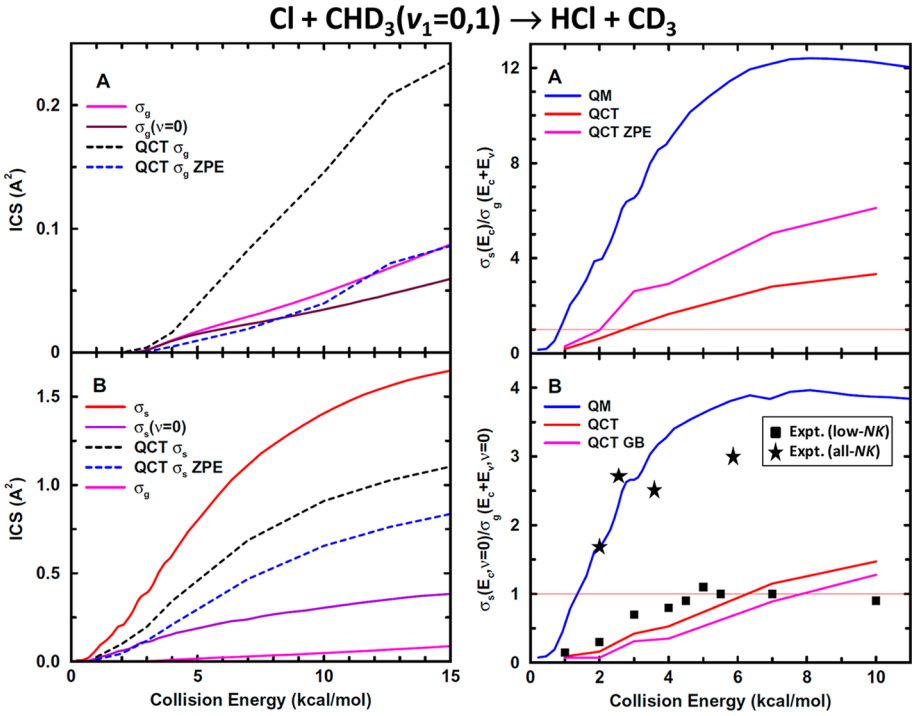

Figure 8. Quantum mechanical and QCT (with and without ZPE constraint) total and the product $CD_3(v = 0)$ cross-sections for the ground-state (g) and CH stretching-excited (s) $Cl + CHD_3(v_1 = 0,1) \rightarrow HCl + CD_3$ reactions (left panels). In the right panels the vibrational enhancement factors of the total (right A) and product $CD_3(v = 0)$ (right B) cross-sections are shown, based on an equivalent amount of total energy, where the vibrational energy E_v is 8.5 kcal/mol. Experimental data corresponding to the low-*NK* and all-*NK* states of $CD_3(v = 0)$ are taken from refs 18 and 106, respectively. Adapted from ref 79.

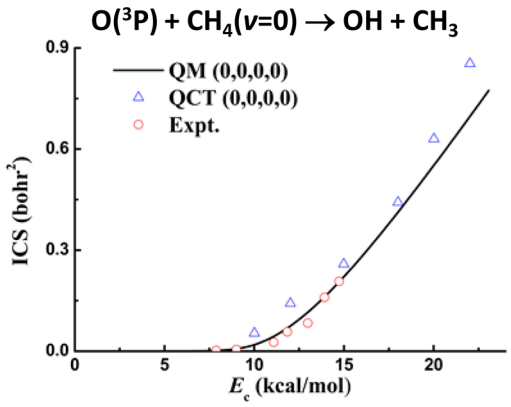

Figure 9. Quantum mechanical (QM) and quasiclassical trajectory (QCT) cross-sections as a function of collision energy for the $O(^3P) + CH_4(v = 0)$ reaction (including the 2/3 degeneracy factor). The QCT results are based on all trajectories without ZPE constraint or weighting. Experimental data are taken from ref 118. Adapted from ref 117.

ZPE constraint, which may affect the QCT data as discussed below.

In Figure 10 the QM ICSs of $O(^3P) + CH_4(v_k = 0,1)$ [$k = 1, 2, 3, 4$] are compared to various QCT data obtained by using different ZPE constraints.[62] As mentioned above, for $O(^3P) + CH_4(v = 0)$ the nonconstrained QCT results agree well with QM. However, several trajectories violate the product ZPE; thus, the soft, CH_3-based, and especially the hard ZPE constrained ICSs underestimate the QM results. Thus, the excellent agreement between the nonconstrained QCT and the QM ICSs may be due to error cancelations; e.g., QCT does not allow tunneling, but allows ZPE leak, which may increase the reactivity due to unphysical energy transfer from the spectator modes to the reaction coordinate. Note that ZPE constraint means discarding trajectories if the sum of the product vibrational energies is less than the sum of ZPEs (soft), either product has less vibrational energy than the corresponding ZPE (hard), and the polyatomic product has less vibrational energy than its ZPE (CH_3 based). For the bending-excited $O(^3P) + CH_4(v_k = 1)$ [$k = 4, 2$] reactions the soft and CH_3-based ZPE constraints give the best agreement with QM, whereas the nonconstrained and hard results overestimate and underestimate the QM results, respectively. For the stretching-excited $O(^3P) + CH_4(v_k = 1)$ [$k = 1, 3$] reactions the nonconstrained and soft constrained ICSs agree well with QM, whereas the CH_3-based results slightly and the hard ICSs significantly underestimate the QM data. On the basis of the above findings it is not straightforward to predict how one should analyze the QCT results if benchmark QM data are not available. Nevertheless, some general conclusions can be drawn. The ZPE constraints do not necessarily improve the nonconstrained QCT ICSs. The hard constraint is too strict and seriously underestimates the ICSs. For the $O(^3P) + CD_4$ reaction a 6D QM study was recently reported using the CB PES, which found good agreement between QM and QCT for some of initial state specific ICSs.[119]

ICSs for the $Br(^2P_{3/2}) + CH_4(v_k = 0,1)$ [$k = 1, 2, 3, 4$] reactions obtained from QCT calculations using the ab initio PES of ref 85 are shown in Figure 11. The reactivity of $Br + CH_4$ is extremely small; the ICSs are about an order of magnitude smaller than those of $O + CH_4$ and about 2 orders of magnitude smaller than the ICSs of $Cl + CH_4$. Similar to $O/Cl + CH_4$, the bending excitations of CH_4 slightly and the stretching excitations significantly enhance the reactivity. The vibrational enhancement factors are much larger for $Br + CH_4$ than those of $O + CH_4$.

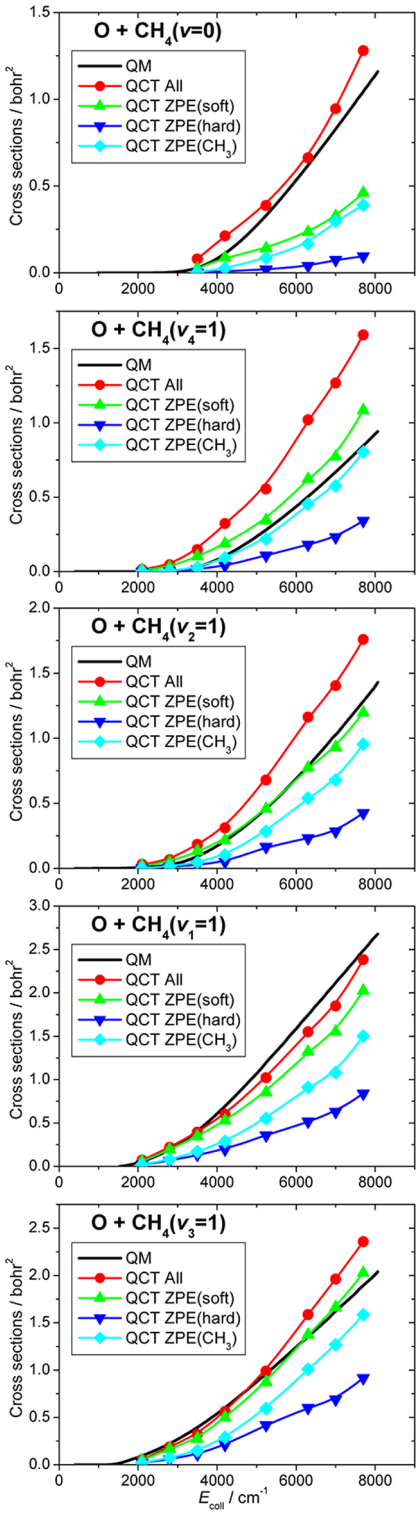

Figure 10. Quantum mechanical (QM) and quasiclassical trajectory (QCT) cross-sections as a function of collision energy for the $O(^3P)$ + $CH_4(v_k = 0, 1)$ [k = 1, 2, 3, 4] reactions. The 8-dimensional QM results are taken from ref 117 (without including the 2/3 degeneracy factor). The QCT data are obtained by considering (a) all trajectories without ZPE constraint or weighting, (b) soft, (c) hard, and (d) CH_3-based ZPE constraints, in which trajectories are discarded if (b) the sum of the product vibrational energies is less than the sum of their ZPEs, (c) either product has less vibrational energy than its ZPE, and (d) the CH_3 product has less vibrational energy than its ZPE. Adapted from ref 62.

The $Br(^2P_{3/2})$ + $CH_4(v_k = 0,1)$ ICSs as a function of total energy (Figure 11) show that the vibrational energy is more efficient than translational energy to activate this late-barrier reaction, in agreement with the extended Polanyi rules. Therefore, Br + CH_4 is a good example where vibrational excitations greatly help the reaction, and for example, Br can react with 2-quantum stretching-excited CH_4 even at low collision energies. Experiments on the dynamics of Br + CH_4 are ongoing in Crim's laboratory. Various ZPE constrained QCT analyses were also done for Br + CH_4 as shown in Figure 11. As seen, the ZPE constraint significantly decreases the ICSs. Unlike for O + CH_4, here QM data are not available yet for comparison. Nevertheless, the different ZPE treatments qualitatively show the same trends for the reactant vibrational effects. Finally, it is worth noting the large difference between the ICSs obtained on the SO and non-SO PESs of Br + CH_4. Even at a high E_{coll} of 16 000 cm^{-1}, the non-SO PES gives about 3 times larger ICS than the SO PES does (Figure 11), showing that the SO correction cannot be neglected in PES developments for heavy atom (Br, I, etc.) reactions.

It is interesting to compare the shapes of the excitation functions of the different reactions. The excitation functions of O/Br + CH_4 have concave-up shapes, whereas Cl + CH_4 shows a concave-down behavior. (Note that the ZPE constraint slightly affects the shapes of the QCT excitation functions.) As discussed by Zhang and Liu,[118] this suggests a tight and loose bending potential near the transition state for O/Br and Cl + CH_4, respectively, which should be investigated in more detail in the near future.

2. Differential Cross-Sections. A joint crossed-beam and QCT study investigated the differential cross-sections (DCSs) of the ground-state and bending-excited Cl + $CH_4(v_b = 0,1)$ reactions.[94] The collision energy dependence of the experimental and theoretical DCSs for $Cl(^2P_{3/2})$ + $CH_4(v = 0)$ is shown in Figure 12. As seen, at a low E_{coll} of 3.7 kcal/mol, the DCS shows significant backward scattering, and as E_{coll} increases, the angular distributions shift toward sideways and forward directions, and at E_{coll} = 20 kcal/mol, the DCS shows clear preference of forward scattering. As Figure 12 shows, experimental and theoretical DCSs are in good qualitative or semiquantitative agreement. The above findings indicate that, at low E_{coll}, Cl + $CH_4(v = 0)$ proceeds with a direct rebound mechanism favoring small impact parameters and thus backward scattering, and as E_{coll} increases, the stripping mechanism starts to dominate favoring larger impact parameters resulting in forward scattering. These conclusions are further supported by the opacity functions as shown in Figure 12. Even if the b_{max} value of about 6 bohr does not significantly depend on E_{coll}, the shape of the opacity function is sensitive to E_{coll}. At low E_{coll}, $P(b)$ decreases monotonically with increasing b, whereas at large E_{coll}, $P(b)$ increases with b up to about b = 4 bohr. The above findings are found to be very similar for the bending-excited reactions as well.

The computed DCSs for the $O(^3P)$ + $CH_4(v_k = 0,1)$ [k = 1, 2, 3, 4] reactions are shown in Figure 13. The shape of the DCSs does not significantly depend on the E_{coll} and the initial vibrational excitation. In a wide E_{coll} range of 3500−7700 cm^{-1} the DCSs of $O(^3P)$ + $CH_4(v = 0)$ show clear preference of backward scattering. This E_{coll} dependence can be contrasted to that of Cl + CH_4, where the angular distributions shifted toward forward directions as E_{coll} increased (Figure 12). These finding indicate that unlike Cl + CH_4, the O + CH_4 reaction occurs with a direct rebound mechanism even at higher collision energies. For $O(^3P)$ + $CH_4(v = 0)$ → $OH(v = 0)$ + $CH_3(v = 0)$, Zhang and

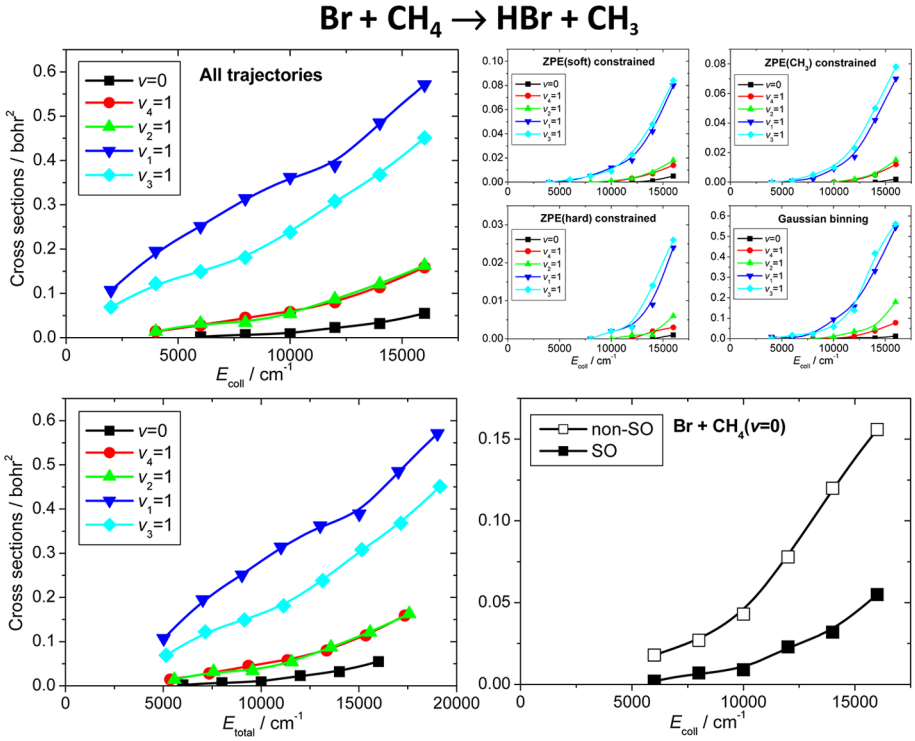

Figure 11. Cross-sections as functions of collision energy (E_{coll}) and total energy (E_{total}) for the ground-state ($v = 0$), bending-excited (v_4 and v_2), and stretching-excited (v_1 and v_3) $Br(^2P_{3/2}) + CH_4(v_k = 0, 1)$ [$k = 1, 2, 3, 4$] reactions obtained by considering all trajectories without ZPE constraint or weighting. For the E_{coll}-dependent cross-sections, results are shown with soft ZPE constraint, hard ZPE constraint, CH_3-based ZPE constraint, and 1GB. In the lower right panel, cross-sections are shown as a function of E_{coll} for the $Br(^2P) + CH_4(v = 0)$ and $Br(^2P_{3/2}) + CH_4(v = 0)$ reactions obtained by using the non-SO and SO PESs, respectively, considering all trajectories without ZPE constraint or weighting. Adapted from ref 85.

Liu[118] measured the angular distributions, which can be directly compared to theory as shown in Figure 14. As seen, both theory and experiment show backward scattering and negligible probabilities in the forward hemisphere. The excellent agreement between theory and experiment confirms the accuracy of the CB PES and shows that QCT is capable to reproduce correlated final state specific DCSs if an accurate PES is used for the simulation.

In 2010 Wang and Liu measured the integral and differential cross-sections of the ground-state and CH stretching excited $O(^3P) + CHD_3(v_1 = 0,1)$ reactions.[20] The measured DCSs show that the ground state reaction is backward scattered, whereas the angular distributions become much broader covering both the backward and forward hemispheres upon CH stretching excitation. This indicates that CH stretching excitation enlarges the reactive cone of acceptance, thereby enhancing the reactivity. In 2012 we performed QCT simulations using the CB PES for the $O(^3P) + CHD_3(v_1 = 0,1)$ reactions.[84] As Figure 15 shows, the reactivity increases significantly upon CH stretching excitation, and the computed DCSs are in excellent agreement with experiment. As also shown in Figure 15, the shape of the computed opacity functions further supports the above interpretation of Wang and Liu since CH stretching excitation enhances the reaction at larger impact parameters, in agreement with the shape of the DCSs. It is interesting to compare the computed DCSs of the $O(^3P) + CH_4(v_1 = 0,1)$ and $CHD_3(v_1 = 0,1)$ reactions. As Figure 13 shows the DCSs of the $O(^3P) + CH_4(v_1 = 0,1)$ reactions do not depend significantly on the vibrational state of CH_4, whereas, as discussed above, the DCS shifts toward forward scattering upon CH stretching excitation of CHD_3. To the best of our knowledge, DCSs have not been measured for the CH stretching excited $O(^3P) + CH_4(v_1 = 1)$ reaction.

The computed reaction probabilities and DCSs for the Br + $CH_4(v_k = 0,1)$ [$k = 1, 2, 3, 4$] reactions are shown in Figure 16.[85] The reactivity of the Br + $CH_4(v = 0)$ reaction is extremely small, for example, the reaction probability at $b = 0$ is only 0.1%. The excitation of the symmetric stretching increases the reactivity, though $P(b = 0)$ is still only 0.8% for Br + $CH_4(v_1 = 1)$. Unlike in the case of $O(^3P) + CH_4$, the DCSs of Br + CH_4 depend on the initial vibrational state. Dominance of backward scattering is found for the Br + $CH_4(v = 0)$ reaction, whereas the bending-excited reactant gives more isotropic angular distributions. For the stretching-excited Br + $CH_4(v_k = 1)$ [$k = 1$ and 3] reactions, the DCSs show dominance of forward scattering. The initial-state dependence of the DCSs is consistent with the b-dependence of the reaction probabilities since b_{max} increases upon reactant vibrational excitation.

3. Vibrational and Rotational Distributions. Computed[82] and measured[120] HF vibrational and rotational distributions for the F + $CH_4(v = 0)$ reaction are shown in Figure 17. Since F + CH_4 is a highly exothermic early barrier reaction, we can expect that the reaction produces vibrationally excited HF molecules. Both theory and experiment show that the major product state is $HF(v = 2)$ and that the $HF(v = 1$ and $3)$ states have minor populations. Note that the ZPE effect is significant on the QCT results since the ZPE constraint decreases the population of $HF(v = 3)$ from 35.0 to 17.5%, thereby improving the agreement with the experimental value of 10.6%.[82] We found that the SO correction does not have a significant effect on the final-state distributions,[87] as shown in Figure 17. The computed rotational distribution is broad for $HF(v = 1)$ and tends colder and colder for $HF(v = 2)$ and $HF(v = 3)$, in excellent agreement with the experiment of Nesbitt and co-workers.[120] Many old

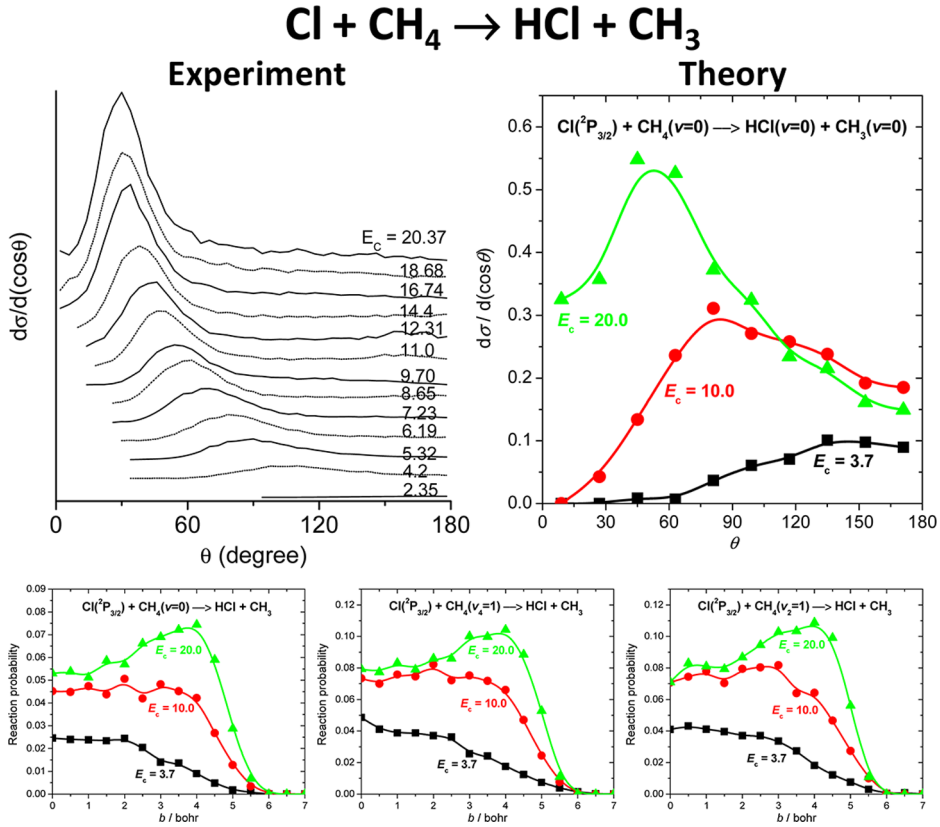

Figure 12. Measured and computed product pair-correlated angular distributions for the $Cl(^2P_{3/2}) + CH_4(v = 0) \rightarrow HCl(v = 0) + CH_3(v = 0)$ reaction (upper panels). The collision energies, E_c, are shown in kcal/mol. Lower panels show the computed reaction probabilities as a function of impact parameter for $Cl(^2P_{3/2}) + CH_4(v = 0)$ and $CH_4(v_b = 1)$ $[b = 4, 2] \rightarrow HCl(\text{all states}) + CH_3(\text{all states})$ at collision energies of 3.7, 10.0, and 20.0 kcal/mol. The QCT results are based on all the trajectories regardless of the internal energy of the products. Adapted from ref 94.

theoretical studies could not reproduce the measured rotational−vibrational distributions. Perhaps the first QCT study that captured the experimental features was reported by Troya in 2005 based on a specific-reaction-parameter semiempirical Hamiltonian.[22] Then in 2009 our QCT study on an ab initio PES finally achieved almost quantitative agreement with experiment as shown in Figure 17.[82]

Computed vibrational distributions for the HCl and CH_3 products of the $Cl(^2P_{3/2}) + CH_4(v = 0)$ reaction are shown in Figure 18. As seen, both HCl and CH_3 are mainly formed in the vibrational ground state. Up to about $E_{coll} = 7000\ cm^{-1}$, the only HCl product state is $v = 0$, and even at a high E_{coll} of 20 000 cm^{-1}, $HCl(v = 0)$ has about 80% population, whereas the fraction of $HCl(v = 1)$ is close to 20% and $HCl(v = 2)$ is still negligible. The mode-specific CH_3 vibrational distributions show that at low collision energies 70−80% of CH_3 is formed in its vibrational ground state, and at $E_{coll} = 20\,000\ cm^{-1}$, the population of $CH_3(v = 0)$ is still about 50%. Umbrella-excited CH_3 is found, $CH_3(v_2 = 1)$ is about 15−20%, and the other product states that have small populations, <10%, are the umbrella overtones, $v_2 = 2$, 3, 4, the bending fundamental $v_4 = 1$, and their combination bands. Stretching-excited CH_3 products are not found. On the basis of the above-described cold HCl and CH_3 vibrational distributions, we can conclude that the excess collision energy mainly transfers into relative translational energy of the products, as expected in the case of a late-barrier reaction.

Mode-specific product vibrational distributions were computed for the $Cl(^2P_{3/2}) + CH_4(v_{4/2} = 0, 1) \rightarrow H + CH_3Cl(n_1n_2n_3n_4n_5n_6)$ reactions using the PES of ref 83, which describes both the abstraction and the high-energy substitution channels.[46] A schematic of the PES for substitution channel and the CH_3Cl vibrational distributions obtained by HB and 1GB are shown in Figure 19. Both HB and 1GB show that the Cl + $CH_4(v = 0)$ reaction produces vibrationally excited CH_3Cl products. However, HB gives small populations for vibrational states that have larger energy than the maximum available energy in the reaction. This can happen due to the breakdown of the normal-mode analysis at highly distorted configurations, which can result in assignments to physically unavailable vibrational states. This issue can be solved by applying 1GB as shown in Figure 19. Indeed, 1GB gives small weights for the states that have much larger quantum energy than the classical total vibrational energy, thereby closing the undesired product states. Similar findings were found for the highly excited $H_2O(n_1n_2n_3)$ product from the reactive quenching of OH* by H_2.[66]

Rotational distributions for the HCl product form the $Cl(^2P_{3/2}) + CH_4(v = 0)$ reaction were measured at $E_{coll} = 1280\ cm^{-1}$ by three different groups.[121−123] The most recent experiment was reported by Orr-Ewing and co-workers,[123] who found very cold rotational distribution, peaking at $J = 1$, in agreement with an earlier experiment of Varley and Dagdigian.[122] Theoretical simulations were struggling to reproduce the measured cold rotational distribution using the QCT method with different PESs and semiempirical Hamiltonians, and instead produced a too-hot rotational distribution. Therefore, in 2011 a study concluded that "...QCT calculations are missing an important dynamical feature that quenches the HCl rotational motion."[51] The conclusion was based on the fact that the HCl

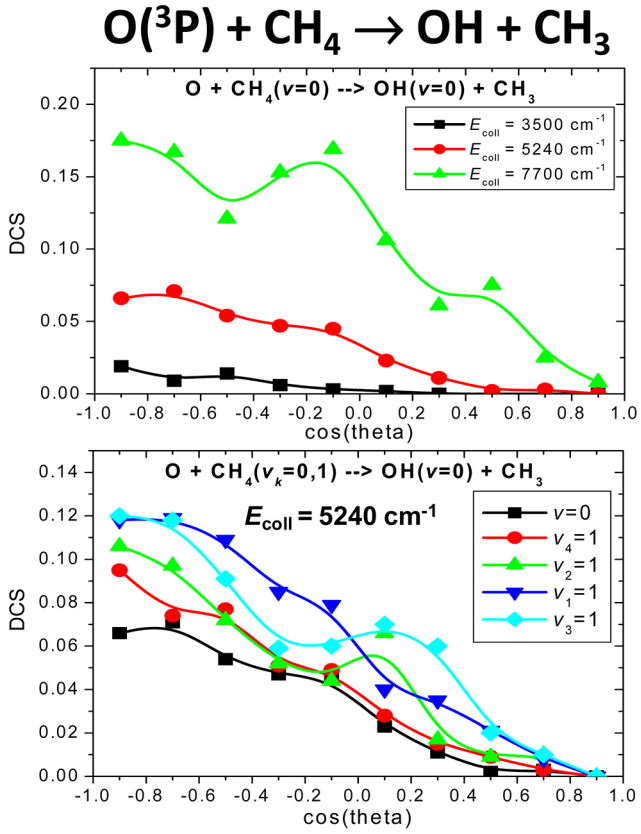

Figure 13. Differential cross-sections (DCSs) for the $O(^3P) + CH_4(v = 0)$ reactions at different collision energies (upper panel) as well as DCSs for the ground-state ($v = 0$), bending-excited (ν_4 and ν_2), and stretching-excited (ν_1 and ν_3) $O(^3P) + CH_4(\nu_k = 0, 1)$ [$k = 1, 2, 3, 4$] reactions at collision energy of 5240 cm^{-1} (lower panel) obtained by considering all trajectories without ZPE constraint or weighting. Adapted from ref 62.

rotational distribution, again quoting from ref 51 "is virtually identical to those obtained with the SRP-MSINDO PES and with the high quality ab initio PES of ref 37." Later in 2011 we performed QCT calculations using the new ab initio PES of ref 83, and the HCl rotational distribution, determined by the same ZPE constrained QCT analysis as was done in ref 51, was obtained in excellent agreement with experiment as shown in Figure 20. As also shown in Figure 20, the rotational distributions are virtually the same with the CH_3-based and soft ZPE constraints; the former was used in refs 83 and 51. Without ZPE constraint, the distribution becomes broader but still peaks at $J = 1$. Trajectory simulations showed that the formation of the CH_3···HCl complex in the exit channel is responsible for producing rotationally cold HCl molecules, in agreement with the findings of Murray and Orr-Ewing,[124] who suggested that the post-transition-state interactions play important roles in the HCl(J) distributions of Cl + alkane reactions.

Computed vibrational distributions for the OH and CH_3 products of the $O(^3P) + CH_4(\nu_k = 0,1)$ [$k = 1, 2, 3, 4$] reactions are shown in Figure 21. For OH(ν), both HB and 1GB QCT results are shown, where in the case of 1GB the weight is obtained as the product of the weights of the product pairs OH and CH_3.[62] Qualitatively, both HB and 1GB show cold OH vibrational distributions, where OH($\nu = 0$) is the dominant product state in a wide E_{coll} range up to at least 7700 cm^{-1}. However, HB gives significantly more OH($\nu = 1$) products than the 1GB results show. This is expected because many CH_3 products violate ZPE; thus, these trajectories may give too high vibrational energy for OH. These unphysical trajectories get small weights when 1GB is applied. 1GB shows that the $O(^3P) + CH_4(\nu = 0)$ reaction gives ground-state OH products only, and OH($\nu = 0$) is still dominant for the stretching excited $O(^3P) + CH_4(\nu_k = 1)$ [$k = 1$ and 3] reactions, where OH($\nu = 1$) has about 20% probability. The mode-specific CH_3 distributions show that the ground-state CH_3 is the dominant product state of the $O(^3P) + CH_4(\nu = 0)$ reaction, in agreement with the crossed-beam experiment of Zhang and Liu,[118] and the minor states include the umbrella- (ν_2) and bending-excited (ν_4) products. The $CH_3(\nu_2)$ vibrational distributions were measured by Suzuki and Hirota,[125] who found monotonically decreasing populations from $\nu_2 = 0$ to 3 and vanishing probability at $\nu_2 = 4$, in excellent agreement with the QCT results of ref 62. QCT shows that no stretching-excited CH_3 is formed from $O(^3P) + CH_4(\nu = 0)$ and even the stretching-excited $O(^3P) + CH_4(\nu_k = 1)$ [$k = 1$ and 3] reactions produce only a few % stretching-excited CH_3. For the umbrella-excited $O(^3P) + CH_4(\nu_4 = 1)$ reaction, Yu and Nyman[71] computed the $CH_3(\nu_2)$ distributions using the RBU quantum model and a semiempirical PES. At high E_{coll} (>5400 cm^{-1}) both the QCT and RBU quantum results show that $CH_3(\nu = 0)$ is the dominant product state. At a lower E_{coll} of 4200 cm^{-1}, QCT shows that $\nu = 0$ and $\nu_2 = 1$ states have the highest populations, whereas the RBU quantum study gives

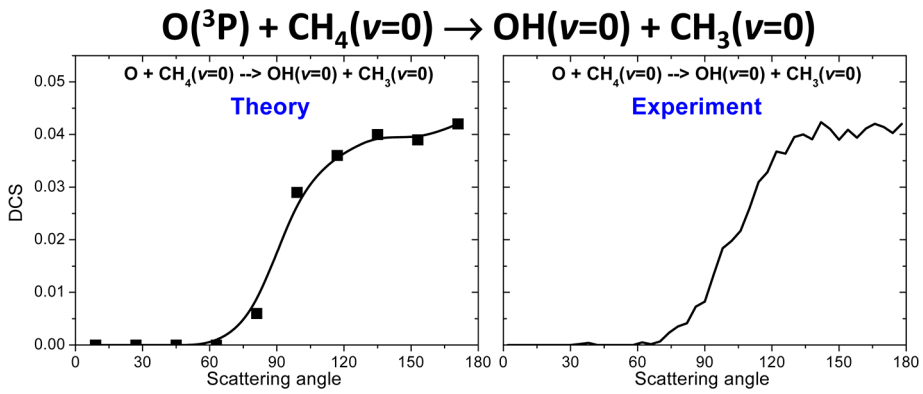

Figure 14. Computed and measured differential cross-sections ($d\sigma/d\cos\theta$) for the $O(^3P) + CH_4(\nu = 0) \rightarrow OH(\nu = 0) + CH_3(\nu = 0)$ reaction at collision energies of 15.0 and 14.7 kcal/mol, respectively. The QCT results are obtained by using histogram binning. The experimental data are taken from ref 118. Adapted from ref 62.

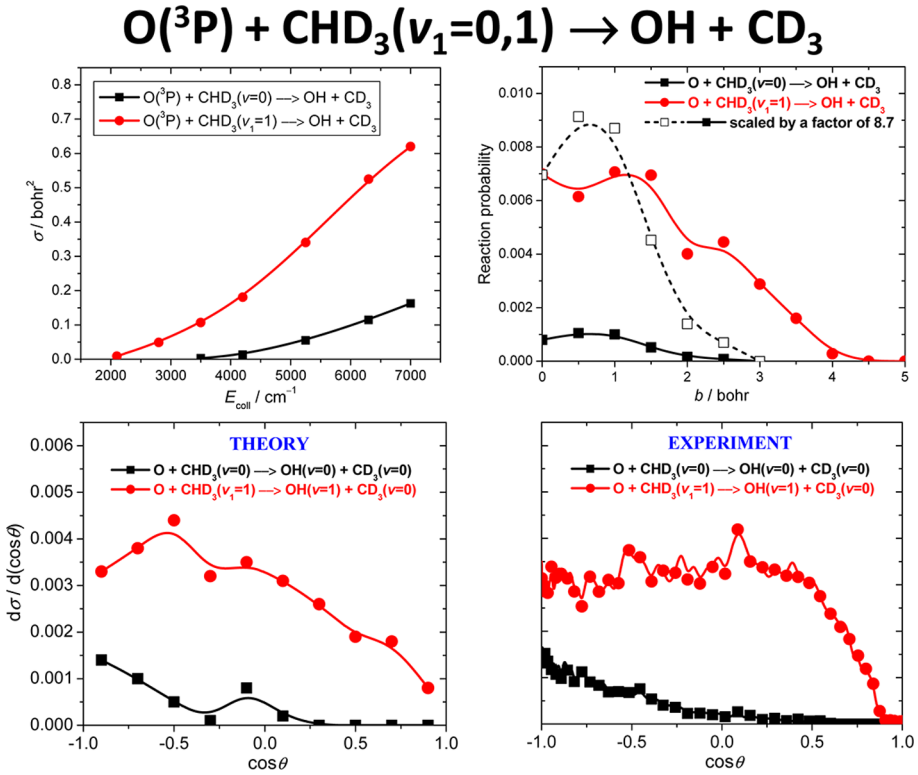

Figure 15. Cross-sections as a function of collision energy and reaction probabilities (E_{coll} = 4000 cm^{-1}) as a function of impact parameter for the ground state and CH stretching excited O(^{3}P) + CHD$_3$(v_1 = 0,1) → OH + CD$_3$ reactions (upper panels, ZPE-constrained QCT results). Computed and measured differential cross-sections of the O(^{3}P) + CHD$_3$(v_1 = 0,1) reactions at collision energy of 4000 cm^{-1} (lower panels). In the QCT analysis, the correlated product-state assignment was done using histogram binning without ZPE constraint. The experimental data are taken from ref 20. Adapted from ref 84.

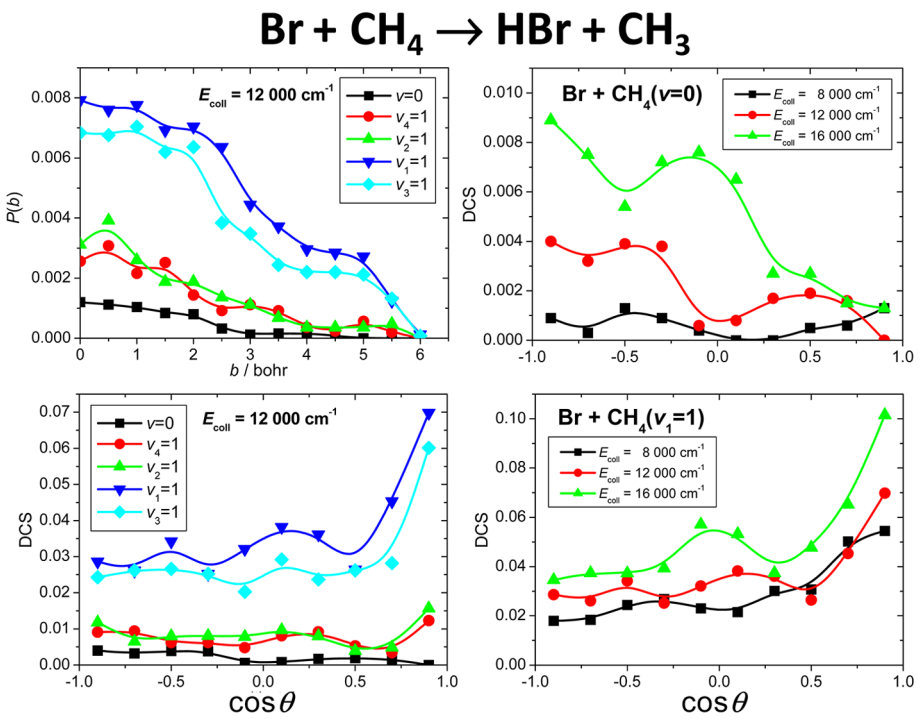

Figure 16. Reaction probabilities as a function of impact parameter (upper left) and differential cross-sections (lower left) for the ground-state (v = 0), bending-excited (v_4 and v_2), and stretching-excited (v_1 and v_3) Br(^{2}P$_{3/2}$) + CH$_4$(v_k = 0, 1) [k = 1, 2, 3, 4] reactions at E_{coll} = 12 000 cm^{-1} obtained by considering all trajectories without ZPE constraint or weighting. In the right panels, differential cross-sections are shown for Br(^{2}P$_{3/2}$) + CH$_4$(v_1 = 0, 1) at three different collision energies. Adapted from ref 85.

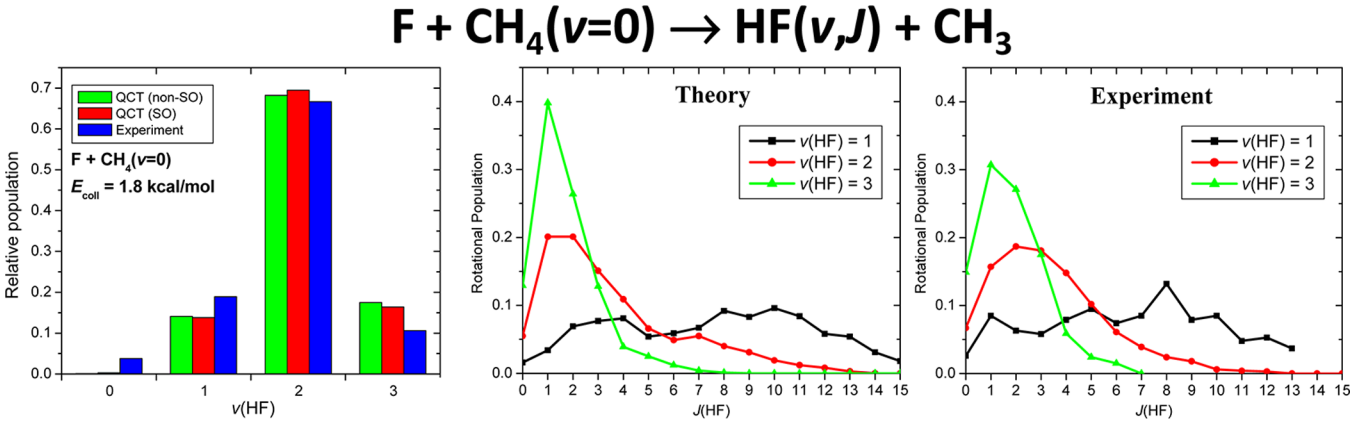

Figure 17. HF vibrational and rotational distributions for the F + CH_4 reaction at collision energy of 1.8 kcal/mol. For the vibrational distributions both the non-SO PES (ref 82) and the SO-corrected PES (ref 87) are used, whereas the rotational distributions are obtained on the non-SO PES. The QCT studies employ ZPE-constrained histogram binning. Theoretical and experimental results are taken from refs 82, 87, and 120, respectively. Adapted from ref 16.

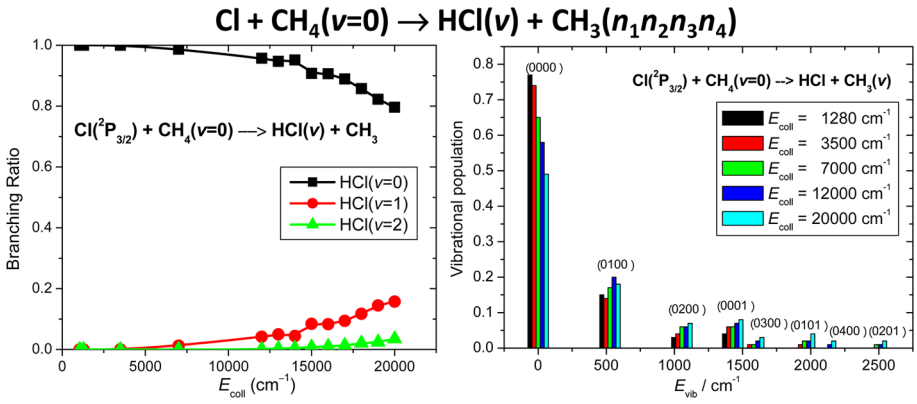

Figure 18. Normalized HCl and mode-specific CH_3 vibrational distributions for the $Cl(^2P_{3/2})$ + $CH_4(v = 0)$ reaction at different collision energies. The QCT study employs histogram binning of $HCl(v)$ considering trajectories in which CH_3 has at least zero-point vibrational energy. The assignment of the vibrational states of CH_3 and their Gaussian binning were done based on ref 45. The harmonic vibrational energies of CH_3 are relative to the ZPE (6548 cm^{-1}). The harmonic frequencies corresponding to the modes (ω_1, ω_2, ω_3, and ω_4) of CH_3 are (3128, 527, 3293, and 1428) cm^{-1}. The states shown here correspond to 98, 99, 97, 97, and 92% of the total CH_3 vibrational populations at collision energies of 1280, 3500, 7000, 12 000, and 20 000 cm^{-1}, respectively. Adapted from ref 61.

hotter vibrational distributions with negligible $CH_3(v = 0)$. Unfortunately, experimental data are not available for the $O(^3P)$ + $CH_4(\nu_4 = 1)$ reaction. Overall, it is found that the $O(^3P)$ + $CH_4(\nu_k = 0,1)$ reactions produce mainly ground-state OH + CH_3 product pairs; thus, the excess translational and/or vibrational energy transfers into relative translational energy of the products.

IV. SUMMARY AND CONCLUSIONS

Moving beyond atom + diatom and atom + triatom reactions, the atom + methane reactions have become benchmark systems of polyatomic abstraction processes. Since methane has nine vibrational modes including torsional motions, which involve the concerted motion of many atoms, the dynamics of the atom + methane reactions is much more complex than that of the tri- and tetra-atomic prototype reactions. In the past decade, experimental techniques were developed to probe the state-to-state dynamics of atom + methane reactions, thereby tracking the energy flow along the reaction coordinate.[15] Of course, detecting all the final states is very challenging; thus, experiment probes the major product states, e.g., the ground state of the methyl product or the umbrella-excited overtones. Theoretically, the simulation of the reactions involves two main steps. First, the potential energy surface (PES) is developed, which governs the motion of the nuclei. Second, dynamical computations are performed using the PES. For the X + methane [X = H, F, $O(^3P)$, Cl, Br] reactions, full-dimensional analytical PESs were developed by (a) a semiempirical approach, calibrating several parameters of the functional form of an old H + CH_4 model PES, and (b) fitting high-level ab initio energies. Our approach follows (b) using the permutationally invariant polynomial approach.[29,16] The PESs are used in full-dimensional QCT and reduced-dimensional quantum mechanical dynamical computations. In order to simulate the product-state specific experiments, a normal-mode analysis method was developed to assign harmonic classical actions to polyatomic product molecules. In 2009 we proposed an efficient method for the application of the Gaussian binning (GB) technique for polyatomic processes, thereby including some quantum effect into the QCT product analysis.[45] This energy-based polyatomic GB method is now called 1GB. 1GB was validated against benchmark quantum results for the OH + D_2 → D + $HOD(n_1n_2n_3)$ reaction, and 1GB has been used for the X + methane reactions, as well. As state-to-state quantum methods improve for six-atom systems, we expect

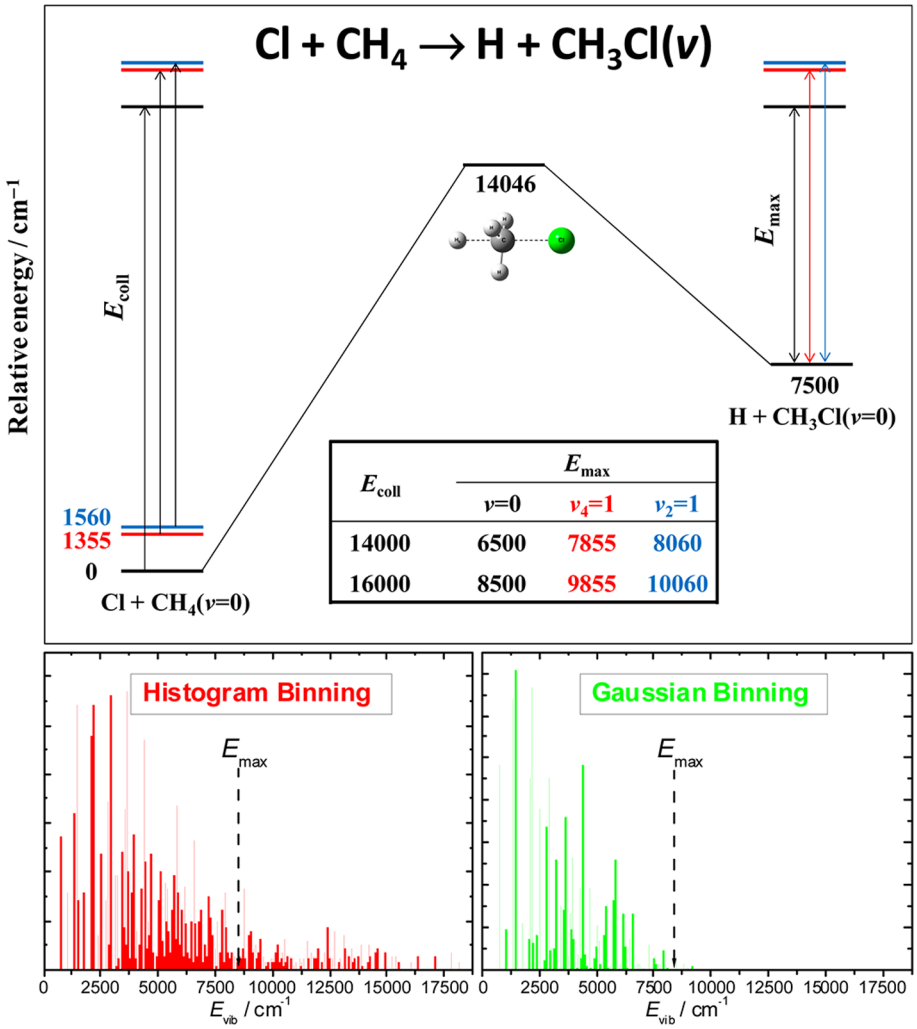

E_{coll}	E_{max}		
	v=0	v_4=1	v_2=1
14000	6500	7855	8060
16000	8500	9855	10060

Figure 19. Schematic of the vibrationally adiabatic potential energy surface of the $Cl(^2P_{3/2}) + CH_4(\nu_{4/2} = 0, 1) \rightarrow H + CH_3Cl$ reactions showing the collision energy (E_{coll}) dependence of the maximal available internal energy (E_{max}) for CH_3Cl at different initial states of the reactant (upper panel). The relative energies correspond to the global PES of refs 83 and 61 including harmonic ZPE corrections. Product CH_3Cl vibrational distributions (showing all the product states) for the $Cl(^2P_{3/2}) + CH_4(v = 0)$ reaction at collision energy of 16 000 cm^{-1} obtained by histogram binning and Gaussian binning (1GB) (lower panels). Adapted from ref 46.

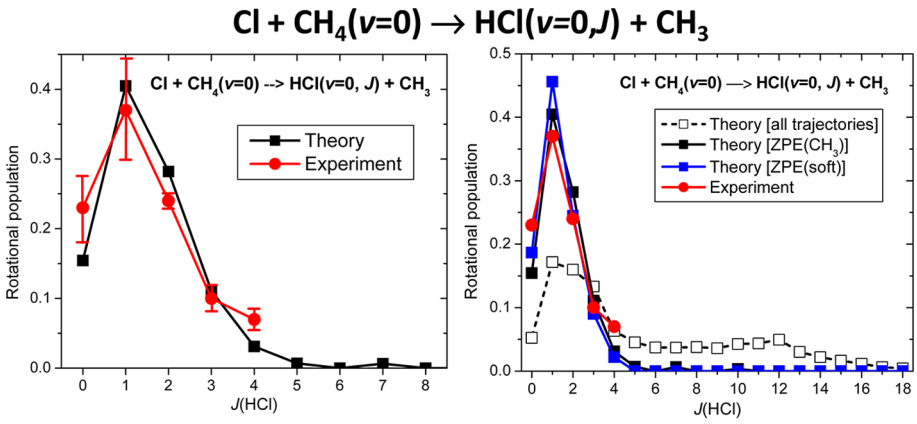

Figure 20. Normalized $HCl(v = 0, J)$ rotational distributions in the $Cl(^2P_{3/2}) + CH_4(v = 0)$ reaction at $E_{coll} = 1280$ cm^{-1}. The QCT study considers all the trajectories, ZPE constrained trajectories in which CH_3 has at least zero-point vibrational energy [ZPE(CH_3)] and ZPE constrained trajectories in which $E_{vib}(HCl) + E_{vib}(CH_3)$ is at least ZPE(HCl) + ZPE(CH_3) [ZPE(soft)]. The experimental results are taken from ref 123. Adapted from refs 83 and 61.

rigorous tests of 1GB for the $X + CH_4$ reactions. Nowadays, state-to-state quantum dynamics computations are usually performed using reduced-dimensional models. Nevertheless, important advances are currently under development for computing

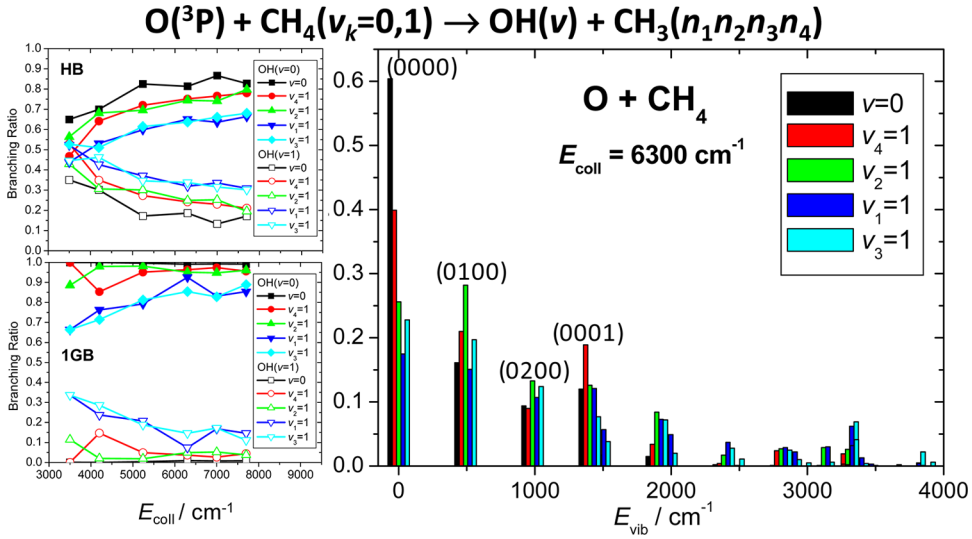

Figure 21. Normalized OH (left) mode-specific CH_3 (right) vibrational distributions for the $O(^3P) + CH_4(\nu_k = 0, 1)$ [$k = 1, 2, 3, 4$] reactions. For OH, the QCT study employs histogram binning (HB) without ZPE constraint and Gaussian binning via the 1GB procedure. For CH_3, 1GB is employed. The harmonic frequencies of CH_3 (ω_1, ω_2, ω_3, and ω_4) are (3118, 491, 3294, and 1403) cm^{-1}. Adapted from ref 62.

full-dimensional state-to-state cross-sections for X + methane reactions using the MCTDH approach.

One of the fundamental questions is concerned about the validity of the extended Polanyi rules for polyatomic reactions. Since the rules were proposed for atom + diatom reactions, it is argued that they may not be simply extended for polyatomic systems. Indeed, Liu and co-workers found departures from our simplified expectations, namely, that CH stretching excitation enhances the D-abstraction in F + CHD_3 and that translational energy is more efficient than CH stretching excitation to activate the late-barrier Cl + CHD_3 reaction.[19,18] QCT simulations showed that the shallow van der Waals well in the entrance channel of the reactions plays an important steering role in the dynamics, which causes the unexpected results. These findings have inspired several experimental and theoretical studies, some of them are still ongoing. In the past 1−2 years, quantum simulations of Cl + CHD_3 found larger vibrational enhancement factors than QCT and experiment.[79] This theoretical study inspired an experimental reinvestigation,[106] which found that probing all the *NK* rotational states of $CD_3(\nu = 0)$ increases the vibrational enhancement relative to the previous study, which probed the low *NK* states only. The new experimental data are in good agreement with the quantum computations. A next question is how the reactant rotational excitations influence the reactivity. Theoretical and experimental work is in progress about this reactant rotational-probe effect. Another question is how this state-to-state dynamical information can be formulated into general rules of polyatomic reactions. As mentioned above, there are several ongoing research projects investigating these questions, and we expect extensive research on this topic in the near future because the story of the extended Polanyi rules has not been ended even for the F and Cl + methane reactions.

Beside the many open questions about the mode-selective dynamics of the X + methane reactions, recent experiments and computations have extended our knowledge on polyatomic reactivity. Let us summarize the most important findings about the X + methane [X = F, $O(^3P)$, Cl, Br] reactions.

(1) F, $O(^3P)$, Cl, and Br + CH_4 are early-barrier−highly exothermic, central-barrier−slightly endothermic, late-barrier−slightly endothermic, and late-barrier−highly endothermic reactions, respectively.

(2) All the X + methane [X = F, $O(^3P)$, Cl, Br] reactions have a shallow vdW well in the entrance channel, where the HCH_3···X minimum is deeper than H_3CH···X, and a relatively stable CH_3···HX complex in the product well.

(3) The reactivity of X + CH_4 decreases in the order of F, Cl, O, and Br.

(4) For F and $O(^3P)$ + methane, translational energy is more efficient than vibrational excitation to promote the reaction. Vibrational energy drives the Cl + methane reaction more efficiently, except at low collision energies. For Br + methane, vibrational energy is clearly more efficient than translational energy to activate the reaction, in agreement with the Polanyi rules.

(5) The angular distributions of Cl + CH_4 shift from backward to forward directions with increasing collision energy indicating the dominance of stripping over the rebound mechanism as collision energy increases. The product angular distributions of $O(^3P)$ + CH_4 show backward scattering without significant collision energy and initial vibrational state dependence. Br + CH_4 is backward scattered for the ground-state reaction, whereas forward dominance is seen upon reactant stretching excitations.

(6) The F + $CH_4(\nu = 0)$ reaction produces inverted HF vibrational distributions, where $HF(\nu = 2)$ is the most populated state, whereas the $O(^3P)$ and Cl + $CH_4(\nu = 0)$ reactions give mainly ground-state $OH(\nu = 0)$ + $CH_3(\nu = 0)$ and $HCl(\nu = 0)$ + $CH_3(\nu = 0)$ product pairs, respectively.

Finally, we emphasize that for most of the above dynamical findings there is good agreement between theory and experiment. Theory can provide explanation of the experimental results and predictions, which may inspire new experiments. Experiment can provide accurate data, which may serve as reference for testing the accuracy of the PESs and dynamical computations. We think that the joint and back-to-back theoretical−experimental efforts will remain the driving force of the field and will uncover many new, perhaps unexpected, details about polyatomic reactivity.

AUTHOR INFORMATION

Corresponding Authors

*(G.C.) E-mail: czako@chem.elte.hu.

*(J.M.B.) E-mail: jmbowma@emory.edu.

Notes

The authors declare no competing financial interest.

Biographies

Gábor Czakó received his Ph.D. in theoretical chemistry at Eötvös University, Budapest, Hungary in 2007. From January 2008 to December 2011 he was a postdoctoral fellow with Professor Joel Bowman in the Department of Chemistry at Emory University, and he is currently a research associate at the Institute of Chemistry, Eötvös University. His research interests involve potential energy surface developments, reaction dynamics computations, first-principles (ro)vibrational spectroscopy, and high-accuracy ab initio thermochemistry. In 2012 he received the Polanyi Prize of the Hungarian Academy of Sciences, given each year to the best Hungarian physical chemist under age 35, and the Junior Prima Prize, which is one of the most prestigious national awards given to the most outstanding Hungarian scientists under age 33.

Joel M. Bowman obtained his A.B. degree in 1969 from the University of California, Berkeley and his Ph.D. degree in 1974 from the California Institute of Technology. He is the Samuel Candler Dobbs Professor of Chemistry at Emory University. He is a Fellow of the American Physical Society and American Association for the Advancement of Science and a member of the International Academy of Quantum Molecular Sciences. He received the Herschbach medal for Theory in 2013. His research interests are reaction and vibrational dynamics and potential energy surfaces.

ACKNOWLEDGMENTS

G.C. was supported by the European Union and the State of Hungary, cofinanced by the European Social Fund in the framework of TÁMOP 4.2.4.A/1-11-1-2012-0001 'National Excellence Program'. G.C. also thanks the Scientific Research Fund of Hungary (OTKA, NK83583) for providing financial support for the computational resources for some of the projects. J.M.B. thanks the Department of Energy (DE-FG02-97ER14782) for financial support. The authors are grateful to the many experimental and theoretical collaborators for the joint work and valuable discussions.

REFERENCES

(1) Schatz, G. C.; Kuppermann, A. Quantum Mechanical Reactive Scattering: An Accurate Three-Dimensional Calculation. *J. Chem. Phys.* **1975**, *62*, 2502−2504.

(2) Schatz, G. C.; Kuppermann, A. Quantum Mechanical Reactive Scattering for Three-Dimensional Atom Plus Diatom Systems. I. Theory. *J. Chem. Phys.* **1976**, *65*, 4642−4667.

(3) Schatz, G. C.; Bowman, J. M.; Kuppermann, A. Exact Quantum, Quasiclassical, and Semiclassical Reaction Probabilities for the Collinear F + H_2 → FH + H Reaction. *J. Chem. Phys.* **1975**, *63*, 674−684.

(4) Persky, A. Quasiclassical Trajectory Studies of the Chlorine−Hydrogen System. I. Cl + H_2 → HCl + H. *J. Chem. Phys.* **1977**, *66*, 2932−2942.

(5) Skouteris, D.; Castillo, J. F.; Manolopoulos, D. E. ABC: A Quantum Reactive Scattering Program. *Comput. Phys. Commun.* **2000**, *133*, 128−135.

(6) Polanyi, J. C. Some Concepts in Reaction Dynamics. *Science* **1987**, *236*, 680−690.

(7) Schatz, G. C.; Colton, M. C.; Grant, J. L. A Quasiclassical Trajectory Study of the State-to-State Dynamics of H + H_2O → OH + H_2. *J. Phys. Chem.* **1984**, *88*, 2971−2977.

(8) Sinha, A.; Hsiao, M. C.; Crim, F. F. Bond-Selected Bimolecular Chemistry: H + HOD($4v_{OH}$) → OD + H_2. *J. Chem. Phys.* **1990**, *92*, 6333−6335.

(9) Bronikowski, M. J.; Simpson, W. R.; Girard, B.; Zare, R. N. Bond-Specific Chemistry: OD:OH Product Ratios for the Reactions H + HOD(100) and H + HOD(001). *J. Chem. Phys.* **1991**, *95*, 8647−8648.

(10) Metz, R. B.; Thoemke, J. D.; Pfeiffer, J. M.; Crim, F. F. Selectively Breaking Either Bond in the Bimolecular Reaction of HOD with Hydrogen Atoms. *J. Chem. Phys.* **1993**, *99*, 1744−1751.

(11) Zhang, D. H.; Light, J. C. Mode Specificity in the H + HOD Reaction. Full-Dimensional Quantum Study. *J. Chem. Soc., Faraday Trans.* **1997**, *93*, 691−697.

(12) Camden, J. P.; Bechtel, H. A.; Zare, R. N. Dynamics of the Simplest Reaction of a Carbon Atom in a Tetrahedral Environment. *Angew. Chem., Int. Ed.* **2003**, *42*, 5227−5230.

(13) Kim, Z. H.; Alexander, A. J.; Bechtel, H. A.; Zare, R. N. Comparison of Near-Threshold Reactivity of Ground-State and Spin-Orbit Excited Chlorine Atoms with Methane. *J. Chem. Phys.* **2001**, *115*, 179−183.

(14) Yoon, S.; Henton, S.; Zivkovic, A. N.; Crim, F. F. The Relative Reactivity of the Stretch−Bend Combination Vibrations of CH_4 in the Cl($^2P_{3/2}$) + CH_4 Reaction. *J. Chem. Phys.* **2002**, *116*, 10744−10752.

(15) Lin, J. J.; Zhou, J.; Shiu, W.; Liu, K. State-Specific Correlation of Coincident Product Pairs in the F + CD_4 Reaction. *Science* **2003**, *300*, 966−969.

(16) Bowman, J. M.; Czakó, G.; Fu, B. High-Dimensional Ab Initio Potential Energy Surfaces for Reaction Dynamics Calculations. *Phys. Chem. Chem. Phys.* **2011**, *13*, 8094−8111.

(17) Manikandan, P.; Zhang, J.; Hase, W. L. Chemical Dynamics Simulations of X^- + CH_3Y → XCH_3 + Y^- Gas-Phase S_N2 Nucleophilic Substitution Reactions. Nonstatistical Dynamics and Nontraditional Reaction Mechanisms. *J. Phys. Chem. A* **2012**, *116*, 3061−3080.

(18) Yan, S.; Wu, Y. T.; Zhang, B.; Yue, X.-F.; Liu, K. Do Vibrational Excitations of CHD_3 Preferentially Promote Reactivity Toward the Chlorine Atom? *Science* **2007**, *316*, 1723−1726.

(19) Zhang, W.; Kawamata, H.; Liu, K. CH Stretching Excitation in the Early Barrier F + CHD_3 Reaction Inhibits CH Bond Cleavage. *Science* **2009**, *325*, 303−306.

(20) Wang, F.; Liu, K. Enlarging the Reactive Cone of Acceptance by Exciting the C−H Bond in the $O(^3P)$ + CHD_3 Reaction. *Chem. Sci.* **2010**, *1*, 126−133.
(21) Wang, F.; Lin, J.-S.; Liu, K. Steric Control of the Reaction of CH Stretch-Excited CHD_3 with Chlorine Atom. *Science* **2011**, *331*, 900−903.
(22) Troya, D. Ab Initio and Direct Quasiclassical-Trajectory Study of the F + CH_4 → HF + CH_3 Reaction. *J. Chem. Phys.* **2005**, *123*, 214305.
(23) Troya, D.; Weiss, P. J. E. Ab Initio and Direct Quasiclassical-Trajectory Study of the Cl + CH_4 → HCl + CH_3 Reaction. *J. Chem. Phys.* **2006**, *124*, 074313.
(24) Collins, M. A. Molecular Potential-Energy Surfaces for Chemical Reaction Dynamics. *Theor. Chem. Acc.* **2002**, *108*, 313−324.
(25) Dawes, R.; Passalacqua, A.; Wagner, A. F.; Sewell, T. D.; Minkoff, M.; Thompson, D. L. Interpolating Moving Least-Squares Methods for Fitting Potential Energy Surfaces: Using Classical Trajectories to Explore Configuration Space. *J. Chem. Phys.* **2009**, *130*, 144107.
(26) Patrício, M.; Santos, J. L.; Patrício, F.; Varandas, A. J. C. Roadmap to Spline-Fitting Potentials in High Dimensions. *J. Math. Chem.* **2013**, *51*, 1729−1746.
(27) Chen, J.; Xu, X.; Xu, X.; Zhang, D. H. A Global Potential Energy Surface for the H_2 + OH ↔ H_2O + H Reaction Using Neural Networks. *J. Chem. Phys.* **2013**, *138*, 154301.
(28) Li, J.; Jiang, B.; Guo, H. Permutation Invariant Polynomial Neural Network Approach to Fitting Potential Energy Surfaces. II. Four-Atom Systems. *J. Chem. Phys.* **2013**, *139*, 204103.
(29) Braams, B. J.; Bowman, J. M. Permutationally Invariant Potential Energy Surfaces in High Dimensionality. *Int. Rev. Phys. Chem.* **2009**, *28*, 577−606.
(30) Bowman, J. M.; Braams, B. J.; Carter, S.; Chen, C.; Czakó, G.; Fu, B.; Huang, X.; Kamarchik, E.; Sharma, A. R.; Shepler, B. C.; Wang, Y.; Xie, Z. Ab-Initio-Based Potential Energy Surfaces for Complex Molecules and Molecular Complexes. *J. Phys. Chem. Lett.* **2010**, *1*, 1866−1874.
(31) Espinosa-García, J.; Bravo, J. L.; Rangel, C. New Analytical Potential Energy Surface for the $F(^2P)$ + CH_4 Hydrogen Abstraction Reaction: Kinetics and Dynamics. *J. Phys. Chem. A* **2007**, *111*, 2761−2771.
(32) Espinosa-García, J.; García-Bernáldez, J. C. Analytical Potential Energy Surface for the CH_4 + $O(^3P)$ → CH_3 + OH Reaction. Thermal Rate Constants and Kinetic Isotope Effects. *Phys. Chem. Chem. Phys.* **2000**, *2*, 2345−2351.
(33) (a) Corchado, J. C.; Truhlar, D. G.; Espinosa-García, J. Potential Energy Surface, Thermal, and State-Selected Rate Coefficients, and Kinetic Isotope Effects for Cl + CH_4 → HCl + CH_3. *J. Chem. Phys.* **2000**, *112*, 9375−9389. (b) Rangel, C.; Navarrete, M.; Corchado, J. C.; Espinosa-García, J. Potential Energy Surface, Kinetics, and Dynamics Study of the Cl + CH_4 → HCl + CH_3 Reaction. *J. Chem. Phys.* **2006**, *124*, 124306.
(34) Espinosa-García, J. Potential Energy Surface for the CH_3 + HBr → CH_4 + Br Hydrogen Abstraction Reaction: Thermal and State-Selected Rate Constants, and Kinetic Isotope Effects. *J. Chem. Phys.* **2002**, *117*, 2076−2086.
(35) Joseph, T.; Steckler, R.; Truhlar, D. G. A New Potential Energy Surface for the CH_3 + H_2 ↔ CH_4 + H Reaction: Calibration and Calculations of Rate Constants and Kinetic Isotope Effects by Variational Transition State Theory and Semiclassical Tunneling Calculations. *J. Chem. Phys.* **1987**, *87*, 7036−7049.
(36) Castillo, J. F.; Aoiz, F. J.; Bañares, L.; Martinez-Nuñez, E.; Fernández-Ramos, A.; Vazquez, S. Quasiclassical Trajectory Study of the F + CH_4 Reaction Dynamics on a Dual-Level Interpolated Potential Energy Surface. *J. Phys. Chem. A* **2005**, *109*, 8459−8470.
(37) Castillo, J. F.; Aoiz, F. J.; Bañares, L. Quasiclassical Trajectory Study of the Cl + CH_4 Reaction Dynamics on a Quadratic Configuration Interaction with Single and Double Excitation Interpolated Potential Energy Surface. *J. Chem. Phys.* **2006**, *125*, 124316.
(38) Meyer, H.-D.; Manthe, U.; Cederbaum, L. S. The Multi-Configurational Time-Dependent Hartree Approach. *Chem. Phys. Lett.* **1990**, *165*, 73−78.
(39) Welsch, R.; Manthe, U. Fast Shepard Interpolation on Graphics Processing Units: Potential Energy Surfaces and Dynamics for H + CH_4 → H_2 + CH_3. *J. Chem. Phys.* **2013**, *138*, 164118.
(40) Suleimanov, Y. V.; Collepardo-Guevara, R.; Manolopoulos, D. E. Bimolecular Reaction Rates from Ring Polymer Molecular Dynamics: Application to H + CH_4 → H_2 + CH_3. *J. Chem. Phys.* **2011**, *134*, 044131.
(41) Li, Y.; Suleimanov, Y. V.; Yang, M.; Green, W. H.; Guo, H. Ring Polymer Molecular Dynamics Calculations of Thermal Rate Constants for the $O(^3P)$ + CH_4 → OH + CH_3 Reaction: Contributions of Quantum Effects. *J. Phys. Chem. Lett.* **2013**, *4*, 48−52.
(42) Hase, W. L. *Encyclopedia of Computational Chemistry*; Wiley: New York, 1998; p 399−407.
(43) Schatz, G. C. A Program for Determining Primitive Semiclassical Eigenvalues for Vibrating/Rotating Nonlinear Triatomic Molecules. *Comput. Phys. Commun.* **1988**, *51*, 135−147.
(44) Corchado, J. C.; Espinosa-García, J. Product Vibrational Distributions in Polyatomic Species Based on Quasiclassical Trajectory Calculations. *Phys. Chem. Chem. Phys.* **2009**, *11*, 10157−10164.
(45) Czakó, G.; Bowman, J. M. Quasiclassical Trajectory Calculations of Correlated Product Distributions for the F + $CHD_3(v_1 = 0, 1)$ Reactions Using an Ab Initio Potential Energy Surface. *J. Chem. Phys.* **2009**, *131*, 244302.
(46) Czakó, G. Gaussian Binning of the Vibrational Distributions for the Cl + $CH_4(v_{4/2} = 0, 1)$ → H + $CH_3Cl(n_1n_2n_3n_4n_5n_6)$ Reactions. *J. Phys. Chem. A* **2012**, *116*, 7467−7473.
(47) Stillinger, F. H.; Weber, T. A. Packing Structures and Transitions in Liquids and Solids. *Science* **1984**, *225*, 983−989.
(48) Czakó, G.; Kaledin, A. L.; Bowman, J. M. A Practical Method to Avoid Zero-Point Leak in Molecular Dynamics Calculations: Applications to the Water Dimer. *J. Chem. Phys.* **2010**, *132*, 164103.
(49) Czakó, G.; Kaledin, A. L.; Bowman, J. M. Zero-Point Energy Constrained Quasiclassical, Classical, and Exact Quantum Simulations of Isomerizations and Radial Distribution Functions of the Water Trimer Using an Ab Initio Potential Energy Surface. *Chem. Phys. Lett.* **2010**, *500*, 217−222.
(50) Czakó, G.; Wang, Y.; Bowman, J. M. Communication: Quasiclassical Trajectory Calculations of Correlated Product-State Distributions for the Dissociation of $(H_2O)_2$ and $(D_2O)_2$. *J. Chem. Phys.* **2011**, *135*, 151102.
(51) Greaves, S. J.; Rose, R. A.; Abou-Chahine, F.; Glowacki, D. R.; Troya, D.; Orr-Ewing, A. J. Quasi-Classical Trajectory Study of the Dynamics of the Cl + CH_4 → HCl + CH_3 Reaction. *Phys. Chem. Chem. Phys.* **2011**, *13*, 11438−11445.
(52) Ch'ng, L. C.; Samanta, A. K.; Czakó, G.; Bowman, J. M.; Reisler, H. Experimental and Theoretical Investigations of Energy Transfer and Hydrogen-Bond Breaking in the Water Dimer. *J. Am. Chem. Soc.* **2012**, *134*, 15430−15435.
(53) Eckart, C. Some Studies Concerning Rotating Axes and Polyatomic Molecules. *Phys. Rev.* **1935**, *47*, 552−558.
(54) Dymarsky, A. Y.; Kudin, K. N. Computation of the Pseudorotation Matrix to Satisfy the Eckart Axis Conditions. *J. Chem. Phys.* **2005**, *122*, 124103.
(55) Bonnet, L.; Rayez, J. C. Quasiclassical Trajectory Method for Molecular Scattering Processes: Necessity of a Weighted Binning Approach. *Chem. Phys. Lett.* **1997**, *277*, 183−190.
(56) Bonnet, L.; Rayez, J. C. Gaussian Weighting in the Quasiclassical Trajectory Method. *Chem. Phys. Lett.* **2004**, *397*, 106−109.
(57) Bañares, L.; Aoiz, F. J.; Honvault, P.; Launay, J.-M. Dynamics of the $S(^1D)$ + H_2 Insertion Reaction: A Combined Quantum Mechanical and Quasiclassical Trajectory Study. *J. Phys. Chem. A* **2004**, *108*, 1616−1628.
(58) Xie, T.; Bowman, J. M.; Duff, J. W.; Braunstein, M.; Ramachandran, B. Quantum and Quasiclassical Studies of the $O(^3P)$ + HCl → OH + $Cl(^2P)$ Reaction Using Benchmark Potential Surfaces. *J. Chem . Phys.* **2005**, *122*, 014301.
(59) Lin, S. Y.; Guo, H.; Lendvay, G.; Xie, D. Effects of Reactant Rotational Excitation on H + O_2 → OH + O Reaction Rate Constant: Quantum Wave Packet, Quasi-Classical Trajectory and Phase Space Theory Calculations. *Phys. Chem. Chem. Phys.* **2009**, *11*, 4715−4721.

(60) Bonnet, L.; Espinosa-García, J. The Method of Gaussian Weighted Trajectories. V. On the 1GB Procedure for Polyatomic Processes. *J. Chem. Phys.* **2010**, *133*, 164108.
(61) Czakó, G.; Bowman, J. M. Accurate Ab Initio Potential Energy Surface, Thermochemistry, and Dynamics of the $Cl(^2P, ^2P_{3/2}) + CH_4 \rightarrow HCl + CH_3$ and $H + CH_3Cl$ Reactions. *J. Chem. Phys.* **2012**, *136*, 044307.
(62) Czakó, G.; Liu, R.; Yang, M.; Bowman, J. M.; Guo, H. Quasiclassical Trajectory Studies of the $O(^3P) + CX_4(v_k = 0, 1) \rightarrow OX(v) + CX_3(n_1n_2n_3n_4)$ [X = H and D] Reactions on an Ab Initio Potential Energy Surface. *J. Phys. Chem. A* **2013**, *117*, 6409−6420.
(63) Sierra, J. D.; Bonnet, L.; González, M. Quasi-Classical Trajectory-Gaussian Binning Study of the $OH + D_2 \rightarrow HOD(v_1',v_2',v_3') + D$ Angle-Velocity and Vibrational Distributions at a Collision Energy of 0.28 eV. *J. Phys. Chem. A* **2011**, *115*, 7413−7417.
(64) Bonnet, L.; Espinosa-García, J.; Corchado, J. C.; Liu, S.; Zhang, D. H. Classical Versus Quantum Vibrational State Distributions for the Benchmark Polyatomic Reaction $OH + D_2$: Checking the Validity of the QCT Method. *Chem. Phys. Lett.* **2011**, *516*, 137−140.
(65) García, E.; Corchado, J. C.; Espinosa-García, J. A Detailed Product Distribution Analysis of Some Potential Energy Surfaces Describing the $OH + CO \rightarrow H + CO_2$ Reaction. *Comput. Theor. Chem.* **2012**, *990*, 47−52.
(66) Conte, R.; Fu, B.; Kamarchik, E.; Bowman, J. M. A Novel Gaussian Binning (1GB) Analysis of Vibrational State Distributions in Highly Excited H_2O from Reactive Quenching of OH* by H_2. *J. Chem. Phys.* **2013**, *139*, 044104.
(67) Császár, A. G.; Mátyus, E.; Szidarovszky, T.; Lodi, L.; Zobov, N. F.; Shirin, S. V.; Polyansky, O. L.; Tennyson, J. First-Principles Prediction and Partial Characterization of the Vibrational States of Water up to Dissociation. *J. Quant. Spectrosc. Radiat. Transf.* **2010**, *111*, 1043−1064.
(68) Child, M. S. Measureable Consequences of a Dip in the Activation Barrier for an Adiabatic Chemical Reaction. *Mol. Phys.* **1967**, *12*, 401−416.
(69) von Horsten, H. F.; Clary, D. C. Reactive Resonances in the $F + CHD_3$ Reaction: A Quantum Dynamics Study. *Phys. Chem. Chem. Phys.* **2011**, *13*, 4340−4356.
(70) Yu, H.-G.; Nyman, G. Three-Dimensional Quantum Scattering Calculations on the $Cl + CH_4 \leftrightarrow HCl + CH_3$ Reaction. *Phys. Chem. Chem. Phys.* **1999**, *1*, 1181−1190.
(71) Yu, H.-G.; Nyman, G. Quantum Dynamics of the $O(^3P) + CH_4 \rightarrow OH + CH_3$ Reaction: An Application of the Rotating Bond Umbrella Model and Spectral Transform Subspace Iteration. *J. Chem. Phys.* **2000**, *112*, 238−247.
(72) Zhang, J. Z. H. The Semirigid Vibrating Rotor Target Model for Quantum Polyatomic Reaction Dynamics. *J. Chem. Phys.* **1999**, *111*, 3929−3939.
(73) Wang, M. L.; Zhang, J. Z. H. Generalized Semirigid Vibrating Rotor Target Model for Atom−Poly Reaction: Inclusion of Umbrella Mode for $H + CH_4$ Reaction. *J. Chem. Phys.* **2002**, *117*, 3081−3087.
(74) Chu, T.; Zhang, X.; Ju, L.; Yao, L.; Han, K.-L.; Wang, M.; Zhang, J. Z. H. First Principles Quantum Dynamics Study Reveals Subtle Resonance in Polyatomic Reaction: The Case of $F + CH_4 \rightarrow HF + CH_3$. *Chem. Phys. Lett.* **2006**, *424*, 243−246.
(75) Wang, D. Y.; Bowman, J. M. A Reduced Dimensionality, Six-Degree-of-Freedom, Quantum Calculation of the $H + CH_4 \rightarrow H_2 + CH_3$ Reaction. *J. Chem. Phys.* **2001**, *115*, 2055−2061.
(76) Palma, J.; Clary, D. C. A Quantum Model Hamiltonian to Treat Reactions of the Type $X + YCZ_3 \rightarrow XY + CZ_3$: Application to $O(^3P) + CH_4 \rightarrow OH + CH_3$. *J. Chem. Phys.* **2000**, *112*, 1859−1867.
(77) Yang, M.; Lee, S.-Y.; Zhang, D. H. Seven-Dimensional Quantum Dynamics Study of the $O(^3P) + CH_4$ Reaction. *J. Chem. Phys.* **2007**, *126*, 064303.
(78) Yang, M.; Zhang, D. H.; Lee, S.-Y. A Seven-Dimensional Quantum Study of the $H + CH_4$ Reaction. *J. Chem. Phys.* **2002**, *117*, 9539−9542.
(79) Zhang, Z.; Zhou, Y.; Zhang, D. H.; Czakó, G.; Bowman, J. M. Theoretical Study of the Validity of the Polanyi Rules for the Late-Barrier $Cl + CHD_3$ Reaction. *J. Phys. Chem. Lett.* **2012**, *3*, 3416−3419.
(80) Liu, S.; Chen, J.; Zhang, Z.; Zhang, D. H. Communication: A Six-Dimensional State-to-State Quantum Dynamics Study of the $H + CH_4 \rightarrow H_2 + CH_3$ Reaction ($J = 0$). *J. Chem. Phys.* **2013**, *138*, 011101.
(81) Czakó, G.; Szabó, I.; Telekes, H. On the Choice of the Ab Initio Level of Theory for Potential Energy Surface Developments. *J. Phys. Chem. A* **2014**, *118*, 646−654.
(82) Czakó, G.; Shepler, B. C.; Braams, B. J.; Bowman, J. M. Accurate Ab Initio Potential Energy Surface, Dynamics, and Thermochemistry of the $F + CH_4 \rightarrow HF + CH_3$ Reaction. *J. Chem. Phys.* **2009**, *130*, 084301.
(83) Czakó, G.; Bowman, J. M. Dynamics of the Reaction of Methane with Chlorine Atom on an Accurate Potential Energy Surface. *Science* **2011**, *334*, 343−346.
(84) Czakó, G.; Bowman, J. M. Dynamics of the $O(^3P) + CHD_3(v_{CH} = 0, 1)$ Reactions on an Accurate Ab Initio Potential Energy Surface. *Proc. Natl. Acad. Sci. U.S.A.* **2012**, *109*, 7997−8001.
(85) Czakó, G. Accurate Ab Initio Potential Energy Surface, Thermochemistry, and Dynamics of the $Br(^2P, ^2P_{3/2}) + CH_4 \rightarrow HBr + CH_3$ Reaction. *J. Chem. Phys.* **2013**, *138*, 134301.
(86) The National Institute of Standards and Technology (NIST). Handbook of Basic Atomic Spectroscopic Data. http://www.nist.gov/pml/data/handbook/.
(87) Czakó, G.; Bowman, J. M. An Ab Initio Spin−Orbit-Corrected Potential Energy Surface and Dynamics for the $F + CH_4$ and $F + CHD_3$ Reactions. *Phys. Chem. Chem. Phys.* **2011**, *13*, 8306−8312.
(88) Westermann, T.; Eisfeld, W.; Manthe, U. Coupled Potential Energy Surface for the $F(^2P) + CH_4 \rightarrow HF + CH_3$ Entrance Channel and Quantum Dynamics of the $CH_4{\cdot}F^-$ Photodetachment. *J. Chem. Phys.* **2013**, *139*, 014309.
(89) Berning, A.; Schweizer, M.; Werner, H.-J.; Knowles, P. J.; Palmieri, P. Spin−Orbit Matrix Elements for Internally Contracted Multireference Configuration Interaction Wavefunctions. *Mol. Phys.* **2000**, *98*, 1823−1833.
(90) Hammond, G. S. A Correlation of Reaction Rates. *J. Am. Chem. Soc.* **1955**, *77*, 334−338.
(91) Alexander, M. H.; Werner, H.-J.; Manolopoulos, D. E. Spin−Orbit Effects in the Reaction of $F(^2P)$ with H_2. *J. Chem. Phys.* **1998**, *109*, 5710−5713.
(92) Che, L.; Ren, Z.; Wang, X.; Dong, W.; Dai, D.; Wang, X.; Zhang, D. H.; Yang, X.; Sheng, L.; Li, G.; Werner, H.-J.; Lique, F.; Alexander, M. H. Breakdown of the Born−Oppenheimer Approximation in the $F + o\text{-}D_2 \rightarrow DF + D$ Reaction. *Science* **2007**, *317*, 1061−1064.
(93) Wu, Y.-T.; Liu, K. Imaging the Pair-Correlated Dynamics and Isotope Effects of the $Cl + CH_2D_2$ Reaction. *J. Chem. Phys.* **2008**, *129*, 154302.
(94) Zhang, B.; Liu, K.; Czakó, G.; Bowman, J. M. Translational Energy Dependence of the $Cl + CH_4(v_b = 0, 1)$ Reactions: A Joint Crossed-Beam and Quasiclassical Trajectory Study. *Mol. Phys.* **2012**, *110*, 1617−1626.
(95) Remmert, S. M.; Banks, S. T.; Harvey, J. N.; Orr-Ewing, A. J.; Clary, D. C. Reduced Dimensionality Spin−Orbit Dynamics of $CH_3 + HCl \leftrightarrow CH_4 + Cl$ on Ab Initio Surfaces. *J. Chem. Phys.* **2011**, *134*, 204311.
(96) Cheng, M.; Feng, Y.; Du, Y.; Zhu, Q.; Zheng, W.; Czakó, G.; Bowman, J. M. Communication: Probing the Entrance Channels of the $X + CH_4 \rightarrow HX + CH_3$ (X = F, Cl, Br, I) Reactions Via Photodetachment of $X^-{-}CH_4$. *J. Chem. Phys.* **2011**, *134*, 191102.
(97) Neumark, D. M. Slow Electron Velocity-Map Imaging of Negative Ions: Applications to Spectroscopy and Dynamics. *J. Phys. Chem. A* **2008**, *112*, 13287−13301.
(98) Yacovitch, T. I.; Garand, E.; Kim, J. B.; Hock, C.; Theis, T.; Neumark, D. M. Vibrationally Resolved Transition State Spectroscopy of the $F + H_2$ and $F + CH_4$ Reactions. *Faraday Discuss.* **2012**, *157*, 399−414.
(99) Westermann, T.; Kim, J. B.; Weichman, M. L.; Hock, C.; Yacovitch, T. I.; Palma, J.; Neumark, D. M.; Manthe, U. Resonances in the Entrance Channel of the Elementary Chemical Reaction of Fluorine and Methane. *Angew. Chem., Int. Ed.* **2014**, *53*, 1122−1126.

(100) Czakó, G.; Braams, B. J.; Bowman, J. M. Accurate Ab Initio Structure, Dissociation Energy, and Vibrational Spectroscopy of the F^--CH_4 Anion Complex. *J. Phys. Chem. A* **2008**, *112*, 7466−7472.
(101) Allen, W. D.; East, A. L. L.; Császár, A. G. In *Structures and Conformations of Non-Rigid Molecules*; Laane, J., Dakkouri, M., van der Veken, B., Oberhammer, H., Eds.; Kluwer: Dordrecht, Netherlands, 1993; p 343.
(102) Császár, A. G.; Allen, W. D.; Schaefer, H. F. In Pursuit of the Ab Initio Limit for Conformational Energy Prototypes. *J. Chem. Phys.* **1998**, *108*, 9751−9764.
(103) (a) Karton, A.; Martin, J. M. L. Comment on: "Estimating the Hartree−Fock Limit from Finite Basis Set Calculations" [Jensen F (2005) Theor Chem Acc 113:267]. *Theor. Chem. Acc.* **2006**, *115*, 330−333. (b) Klopper, W.; Kutzelnigg, W. Gaussian Basis Sets and the Nuclear Cusp Problem. *J. Mol. Struct.* **1986**, *135*, 339−356. (c) Tasi, G.; Császár, A. G. Hartree−Fock-Limit Energies and Structures with a Few Dozen Distributed Gaussians. *Chem. Phys. Lett.* **2007**, *438*, 139−143.
(104) Helgaker, T.; Klopper, W.; Koch, H.; Noga, J. Basis-Set Convergence of Correlated Calculations on Water. *J. Chem. Phys.* **1997**, *106*, 9639−9646.
(105) Douglas, M.; Kroll, N. M. Quantum Electrodynamical Corrections to the Fine Structure of Helium. *Ann. Phys.* **1974**, *82*, 89−155.
(106) Wang, F.; Lin, J.-S.; Cheng, Y.; Liu, K. Vibrational Enhancement Factor of the Cl + $CHD_3(v_1 = 1)$ Reaction: Rotational-Probe Effects. *J. Phys. Chem. Lett.* **2013**, *4*, 323−327.
(107) Meng, F.; Yan, W.; Wang, D. Y. Quantum Dynamics Study of the Cl + CH_4 → HCl + CH_3 Reaction: Reactive Resonance, Vibrational Excitation Reactivity, and Rate Constants. *Phys. Chem. Chem. Phys.* **2012**, *14*, 13656−13662.
(108) Berke, A. E.; Volpa, E. H.; Annesley, C. J.; Crim, F. F. The Influence of Translational and Vibrational Energy on the Reaction of Cl with CH_3D. *J. Chem. Phys.* **2013**, *138*, 224306.
(109) Jiang, B.; Guo, H. Relative Efficacy of Vibrational vs. Translational Excitation in Promoting Atom−Diatom Reactivity: Rigorous Examination of Polanyi's Rules and Proposition of Sudden Vector Projection (SVP) Model. *J. Chem. Phys.* **2013**, *138*, 234104.
(110) Czakó, G.; Shuai, Q.; Liu, K.; Bowman, J. M. Communication: Experimental and Theoretical Investigations of the Effects of the Reactant Bending Excitations in the F + CHD_3 Reaction. *J. Chem. Phys.* **2010**, *133*, 131101.
(111) Jiang, B.; Guo, H. Control of Mode/Bond Selectivity and Product Energy Disposal by the Transition State: X + H_2O (X = H, F, $O(^3P)$, and Cl) Reactions. *J. Am. Chem. Soc.* **2013**, *135*, 15251−15256.
(112) Jiang, B.; Liu, R.; Li, J.; Xie, D.; Yang, M.; Guo, H. Mode Selectivity in Methane Dissociative Chemisorption on Ni(111). *Chem. Sci.* **2013**, *4*, 3249−3254.
(113) Jiang, B.; Guo, H. Mode and Bond Selectivities in Methane Dissociative Chemisorption: Quasi-Classical Trajectory Studies on Twelve-Dimensional Potential Energy Surface. *J. Phys. Chem. C* **2013**, *117*, 16127−16135.
(114) Troya, D.; Pascual, R. Z.; Schatz, G. C. Theoretical Studies of the $O(^3P)$ + Methane Reaction. *J. Phys. Chem. A* **2003**, *107*, 10497−10506.
(115) González, M.; Hernando, J.; Millán, J.; Sayós, R. Ab Initio Ground Potential Energy Surface, VTST and QCT Study of the $O(^3P)$ + $CH_4(X\,^1A_1)$ → $OH(X\,^2\Pi)$ + $CH_3(X\,^2A_2'')$ Reaction. *J. Chem. Phys.* **1999**, *110*, 7326−7338.
(116) Martinez, R.; Enriquez, P. A.; Puyuelo, M. P.; Gonzalez, M. Dynamics of the $O(^3P)$ + CH_4 → OH + CH_3 Reaction Is Similar to That of a Triatomic Reaction. *J. Phys. Chem. A* **2012**, *116*, 5026−5029.
(117) Liu, R.; Yang, M.; Czakó, G.; Bowman, J. M.; Li, J.; Guo, H. Mode Selectivity for a "Central" Barrier Reaction: Eight-Dimensional Quantum Studies of the $O(^3P)$ + CH_4 → OH + CH_3 Reaction on an Ab Initio Potential Energy Surface. *J. Phys. Chem. Lett.* **2012**, *3*, 3776−3780.
(118) Zhang, B.; Liu, K. Imaging the Reaction Dynamics of the $O(^3P)$ + CH_4 → OH + CH_3 Reaction. *Chem.−Asian J.* **2011**, *6*, 3132−3136.
(119) Yan, W.; Meng, F.; Wang, D. Y. Quantum Dynamics Study of Vibrational Excitation Effects and Energy Requirement on Reactivity for the O + CD_4/CHD_3 → OD/OH + CD_3 Reactions. *J. Phys. Chem. A* **2013**, *117*, 12236−12242.
(120) Harper, W. W.; Nizkorodov, S. A.; Nesbitt, D. J. Quantum State-Resolved Reactive Scattering of F + CH_4 → $HF(v,J)$ + CH_3: Nascent $HF(v,J)$ Product State Distributions. *J. Chem. Phys.* **2000**, *113*, 3670−3680.
(121) Simpson, W. R.; Rakitzis, T. P.; Kandel, S. A.; Lev-On, T.; Zare, R. N. Picturing the Transition-State Region and Understanding Vibrational Enhancement for the Cl + CH_4 → HCl + CH_3 Reaction. *J. Phys. Chem.* **1996**, *100*, 7938−7947.
(122) Varley, D. F.; Dagdigian, P. J. Product State Distributions and Angular Differential Cross Sections from Photoinitiated Reactions of Chlorine Atoms with Small Hydrocarbons. *J. Phys. Chem.* **1995**, *99*, 9843−9853.
(123) Murray, C.; Retail, B.; Orr-Ewing, A. J. The Dynamics of the H-Atom Abstraction Reactions between Chlorine Atoms and the Methyl Halides. *Chem. Phys.* **2004**, *301*, 239−249.
(124) Murray, C.; Orr-Ewing, A. J. The Dynamics of Chlorine-Atom Reactions with Polyatomic Organic Molecules. *Int. Rev. Phys. Chem.* **2004**, *23*, 435−482.
(125) Suzuki, T.; Hirota, E. Vibrational Distribution of CH_3 Produced by the Reaction of $O(^1D_2)$ Atom with CH_4. *J. Chem. Phys.* **1993**, *98*, 2387−2398.